Final Report on Airborne Electromagnetic Geophysical (AEM) Study along the I-80 Corridor and Municipal Wellfields within Albany County near Laramie, WY

July 2021

-Ms. Eva Smith, Geophysicist, M.Sc. Candidate student, Dept. of Geology and Geophysics, University of Wyoming

-Dr. Brad Carr, Geophysicist, Associate Research Scientist, Dept. of Geology and Geophysics, University of Wyoming

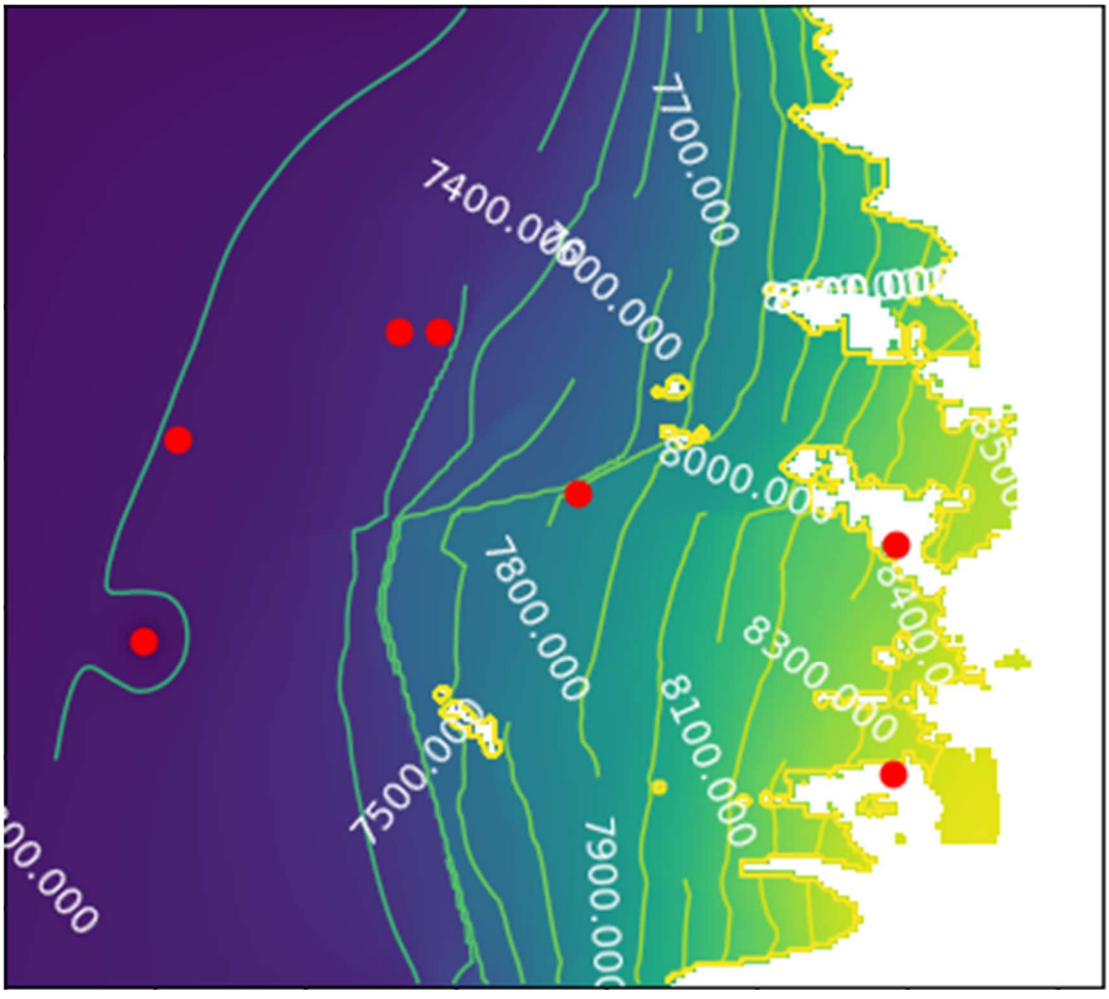

Executive Summary:

The Casper Aquifer is the majority source of groundwater for the municipality of Laramie, WY and surrounding Albany County residents. The rocks that make up this aquifer are both permeable and porous, allowing water to be stored and move within them. Additionally, fracturing and faulting from geologic processes have created more pathways through which water can flow. The danger to this groundwater system has been studied for many years, with concerns for spills on Interstate 80 being one of the points of major concern. Previous studies give necessary background information for our understanding of how water moves through the aquifer, however these data points are few and far between leaving room for error in the interpolation and interpretation of these data. To address this issue of data sparsity, an airborne geophysical survey was flown in October, 2019. These data map electrical resistivity distributions with depth. The subsurface electrical resistivity is correlated to various groundwater parameters of the aquifer such as: water content, porosity and permeability. To understand and predictively model the groundwater flow relative to recharge and potential threats to the Casper Aquifer, it is necessary to get information about these hydraulic parameters in between known wells. This report describes the process through which these airborne geophysical data were transformed into a groundwater flow model. The overall goal of this study is to integrate new geophysical data with existing geologic and hydrologic knowledge of the Casper Aquifer to better understand the flow of groundwater within the exposed section of the Casper and Fountain Formations. This improved understanding will help to create more informed plans to protect the City of Laramie and surrounding Albany County residents' water sources from possible spills on Interstate 80.

During the first year of this study, the airborne electromagnetic (AEM) and airborne magnetic (aeromag) data were collected. The AEM data were processed for noise and inverted to create a smooth 3D model of resistivity throughout the survey area. These data provided a new understanding of the depths to laterally extensive layers that allow for more water movement within the aquifer than others. The aeromag data helped expand our understanding of the relationship between deep structure underlying the Casper Aquifer, and groundwater pathways within and between these laterally extensive layers.

In the second year of the project, the AEM data were transformed into a hydrogeophysical model by picking layers where there were sharp changes in resistivity with depth. These hydrogeophysical layers, HL1 – HL4 from top to bottom respectively, represent bulk sections of the Casper and Fountain formations, generally: HL1 corresponds to Casper Fm. Epsilon, Delta, and into the Gamma member, HL2 encompasses the lower Gamma and top of Beta, HL3 represents the rest of Beta and top of Alpha, and HL4 incorporates middle Alpha through base of the Fountain Formation. Elevations of these hydrogeophysical layers allow bulk resistivities for each 50 m grid cell to be averaged. Since resistivity is correlated to water content and

permeability, these average hydrogeophysical layer resistivities help to define how easily water can move through each layer in the groundwater flow model with the relationships as follows: resistivity below 325 Ωm = 3.55 horizontal ft/day and 0.15 vertical ft/day, resistivity between 325 Ωm and 600 Ωm = 0.56 horizontal ft/day and 0.1 vertical ft/day, and resistivity above 600 Ωm = 0.1 horizontal ft/day and 0.05 vertical ft/day. Hydrogeophysical layers HL2 – HL4 are next incorporated into a groundwater flow model. HL1 is not included in the groundwater modeling effort as it is assumed that this overlying, more resistive layer corresponds to the unsaturated zone of the Casper Formation. Additional lower permeability cells are added where large faults exist within the groundwater model domain. The amount of recharge added to the model was much larger in the more elevated regions of the model than closer to the valley floor. This is assumed to be due to evapotranspiration and the larger distance from land surface to water table. The combination of all these factors allowed a groundwater flow model to be created that closely matched historic water level measurements at monitoring wells and at elevations of two perennial springs. Finally, particle tracking was run on the model to understand from where the Soldier Springs well draws water and how particles released near the interstate corridor would flow if they reached the water table.

Three main conclusions are made from the culmination of this geophysical and hydrologic modeling effort of the Casper Aquifer:

1) Geologic structure has two major influences on how water flows within the aquifer. First, deep topographic changes underlying the Casper Aquifer result in decreased electrical resistivity, which are interpreted as areas of increased vertical and horizontal water movement within the aquifer. Second, surface mapped faults are generally correlated to areas with increases in electrical resistivity, which are interpreted as areas of lower horizontal water movement. However, these faults do not lead to decreases in vertical water movement, indicating these faults allow more water movement between layers. These interpretations of how water moves near large structures within the aquifer inform our understanding of groundwater movement in areas outside of the groundwater model domain.

2) Flow paths from the MODFLOW modeling effort suggests that at current pumping rates, the Soldier Springs well is not vulnerable to spills on the Interstate. However, tracking the direction of flow from particles released near the Interstate shows that Albany County residents, especially between mile markers 317 and 318/319 might bear the brunt of a spill.

3) Recharge to the aquifer is dominant in the more elevated regions of the study area - little water or snowmelt at the surface near the bottom of the interstate 80 corridor reaches the water table. This is good news for spills on the Interstate, as it suggests that contaminants would be unlikely to infiltrate enough of the unsaturated portion of the aquifer to reach the water table. However, due to the varying densities of possible contaminants, their infiltration into the unsaturated zone is most likely different than that of water. A groundwater transport

model would best predict how common contaminants might infiltrate and move through the aquifer.

Transforming borehole and airborne geophysical data into a groundwater model created a better understanding of how water enters, moves through, and exits our local aquifer system. This study showed the relative safety of Soldier Springs from pumping contaminants near the Interstate 80 corridor, and that little precipitation in the lower regions of the mountain front reaches the water table.

Introduction and Background:

Numerous studies to date have been completed to better understand the lithology and groundwater flow dynamics of the Casper Aquifer in the vicinity of Laramie, WY (Huntoon, 1985; Huntoon & Lundy, 1979; Casper Aquifer Protection Plan, 2008). The Casper and underlying Fountain formation, which make up the larger Casper Aquifer supplies 60 percent of municipal water to the City of Laramie and 100 percent to residents in the surrounding Albany County area (Casper Aquifer Protection Plan, 2008). Understanding how water moves through this aquifer in the exposed and unconfined part of the system is extremely important for the creation of a more comprehensive aquifer protection plan. Earlier studies provide necessary background information for our understanding of how water moves through the mountain front of our municipal aquifer, however, with data points few and far between, large uncertainty exists between these points. To address this issue of sparse data, the City of Laramie and Albany County Board of Commissioners jointly funded an airborne geophysical study to characterize the major groundwater flow pathways within the aquifer system.

In the first year of this project airborne electromagnetic (AEM) and airborne magnetic (aeromag) data were collected along east-west flight lines with 100 m spacing, with eight north-south tie lines flown to spatially connect the dense lines of data (Figure 1.). Data were extensively processed to remove noise, such as anthropogenic sources from powerlines and fences. Once the data was considered “noise-free,” a spatially constrained inversion (SCI) was run on all remaining data, which creates a smooth inversion that allows continuity between nearby data points during the inversion (Viezzoli, Christiansen, Auken, & Sørensen, 2008). The aeromag data allows the type of rock beneath the aquifer to be investigated. The broad range in the residual magnetic field show that there exist two main types of rock in the basement underlying the aquifer. Differing rock types indicate areas where structural changes exist in both the basement and overlying layers, which results in increased groundwater flow pathways. For more detailed information on the work accomplished in year one, please see the interim report (Carr & Smith, 2020).

In the second year of the project, all data were cohesively combined, interpreted, and integrated into a groundwater flow model. First, the finalized SCI inverted AEM data and geophysical logs were imported into software GeoScene3D. The geophysical logs allow depths to AEM resistivities to be compared to “ground-truthed” geophysical, hydrologic, and geologic properties, which shows that areas of low electrical resistivity correspond to zones of increased water movement and permeability rather than higher clay content. GeoScene3D was next used to manually and algorithmically pick distinct hydrogeophysical layers that exist in the AEM data (Figure 2). These picked layers were then exported on a 50 m grid across the survey area, giving an elevation for each hydrogeophysical layer every 50 m. For clarity, each hydrogeophysical layer observed in the Casper Fm. will be referred to as HL1 - HL4 from surface to the top of the

Sherman granite bedrock, respectively, for the rest of the report (Figure 2). Using programming language, MATLAB, bulk resistivity values are averaged at each grid point within each layer HL1 - HL4, creating resistivity layers throughout the survey area (Figure 3). The average resistivities for layers HL2 - HL4 are used to constrain the hydraulic properties of the groundwater flow model since lower electrical resistivity correlates to higher hydraulic conductivity (K).

USGS FloPy software was used to construct and easily alter starting conditions, boundary conditions, and hydraulic properties in the groundwater flow model, which was run using USGS MODFLOW 6 (Bakker et al., 2016, 2021). Elevations and resistivities of layers HL1 – HL4 were extrapolated to a larger grid, then directly incorporated into a groundwater flow model, with each layer topography defining groundwater flow layers within the model, and average resistivities within each of the hydrogeophysically significant layers (HL2 - HL4) translated into hydraulic conductivity values. HL1 resistivity is not incorporated into the model since this layer is assumed to be above the water table. Figure 4. shows the extent of each of the hydrogeophysical layers within the groundwater model. As the Casper Fm. outcrops along the mountain front, the hydrogeophysical layers also "disappear," leaving HL3 then HL4 as uppermost layer in the groundwater model. Extrapolating the data to a larger grid was necessary to decrease chances of boundary conditions affecting the groundwater flow in the area of interest. Major mapped faults are added into the groundwater flow model as low hydraulic conductivity, barriers to lateral flow. These faults were especially necessary to replicate hydraulic heads at the Interstate-80 monitoring wells and Klein Springs. Precipitation to each uppermost "on" grid cell, hydraulic conductivities, and boundary conditions were carefully altered until a groundwater flow model most closely representing historic hydraulic head values in the Pope Springs, I-80, and Government Gulch monitoring wells, as well as hydraulic head values similar to ground surface elevation at Klein and Telephone Springs. Replication of the Pope Springs and I-80 hydraulic head values was prioritized to best understand groundwater flow between potential spill sites in I-80 and the municipal sources of groundwater.

This report focuses on three distinct models: Model One (M1) has both low permeability faults and pumping in Soldier Springs and privately owned wells, Model Two (M2) has low permeability faults but no pumping, and Model Three (M3) has neither faults nor pumping. M1 and M2 show how pumping effects the flow of water within the model. M3 demonstrates the importance of having low permeability faults within the model. The flow paths shown in Figure 21. show our understanding of how contaminant spills on the interstate might flow within the aquifer. The amount of work undertaken to create a groundwater model that sufficiently represents known hydraulic head data did not allow time for additionally creating a groundwater transport model. However, since the modeling effort used open source code and

software USGS FloPy and USGS MODFLOW 6, model M1 can be converted to a groundwater transport model.

M1 and M2 have hydraulic head values that are very similar to each other, suggesting the pumping has a relatively small impact on the overall hydraulic head levels in the system. However, when comparing M1 and M2 with M3, it is evident that the addition of low K faults creates a groundwater model that more closely represents observed hydraulic head levels. Seen in Figures 12-16, modeled hydraulic head levels are too high at the I-80 monitoring Pope Springs Wells, and too low at the Government Gulch Wells and Klein and Telephone Springs if low K faults are not added to the groundwater model. Recharge is largely added only in the high elevation areas of the model domain, indicating that very little precipitation along the mountain front of the Casper Aquifer reaches the water table (Figure 7). This is important because it suggests that fluids spilled at the surface along the lower section of the I-80 corridor have a low likelihood of reaching the water table and low potential of reaching the Soldier Springs wellfield.

Figures Figure 20. and Figure 21. are created using USGS MODPATH, which tracks particle movement within an already established USGS MODFLOW 6 model (Bakker et al., 2021; Pollock, 2016). MODPATH is run on M1 to demonstrate where water flows within the aquifer, and the danger spills on the interstate pose to both the city pumping wells and privately owned wells within the model domain. Figure 20. shows the extent from which city well field, Soldier Springs, draws its water with current pumping rates averaged over the past ten years. This figure shows that the particles drawn into the well do not extend to the interstate corridor, suggesting that spills on the interstate have a low likelihood of reaching the municipal well fields. Figure 21 additionally supports this by showing where particles released on and near the interstate corridor flow within the model. However, as seen by the flow paths in Figure 21., this leaves the privately owned wells, shown as black dots, very vulnerable to spills should they reach the water table.

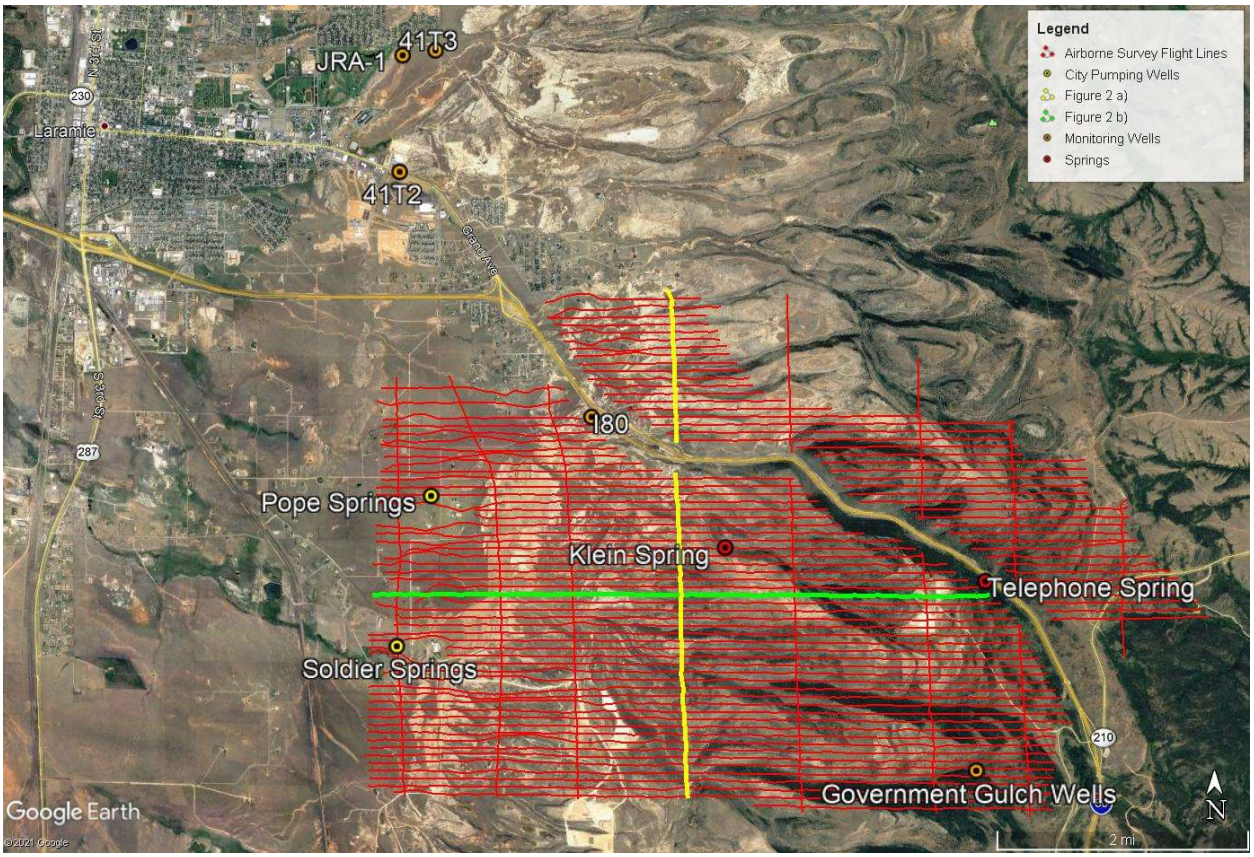

Figure 1.
Map view of AEM and aeromagnetic flight lines, city pumping wells, Pope and Soldier Springs, labeled in yellow, monitoring wells labeled in orange, and perennial springs labeled in red. Yellow and green highlighted flight lines are a) and b) in Figure 2, respectively.

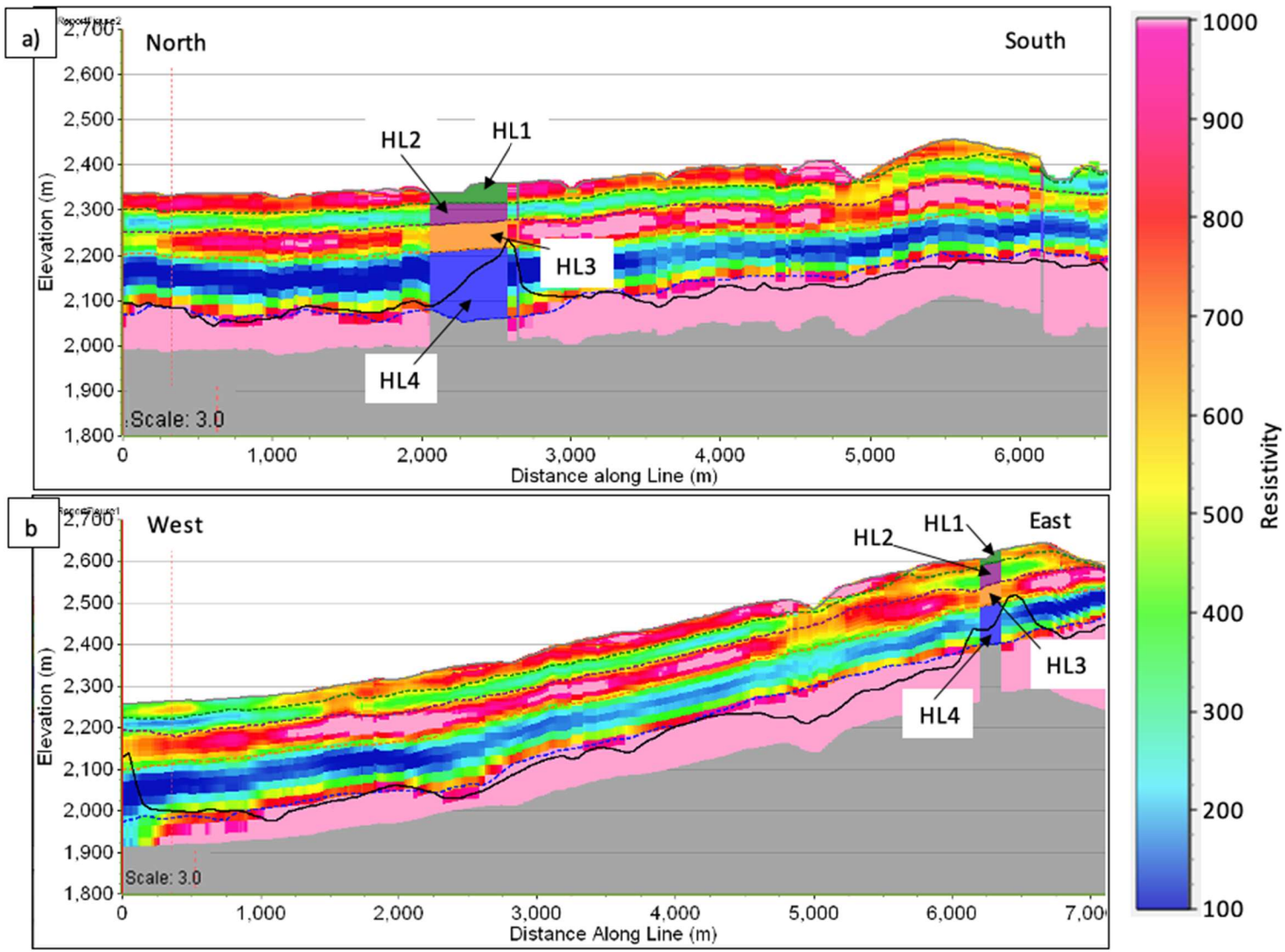

Figure 2.

AEM profiles with algorithmically and manually chosen hydrogeophysical layers, and depth of investigation (DOI) shown as a solid black line. HL1 is shown in green between topography and dashed green line, HL2 in purple between dashed green and purple lines, HL3 in orange between dashed purple and orange lines, and HL4 in blue between dashed orange and blue lines. a) Section from north to south shown in yellow in Figure 1, b) section from west to east shown in green in Figure 1.

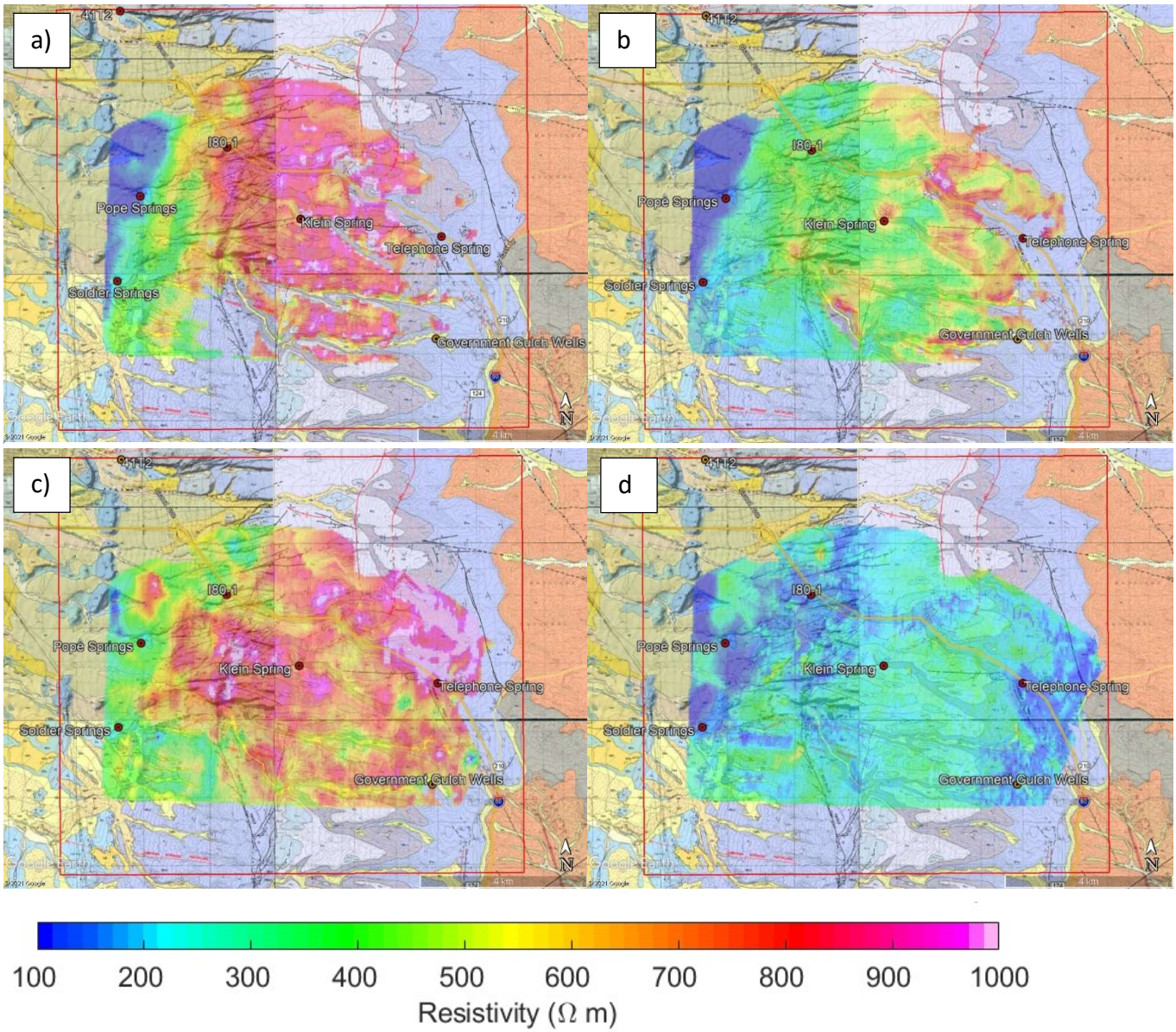

Figure 3.

Geologic map and average resistivities (Ωm) per 50 m grid cell within each hydrogeophysical layer (HL1- HL4) overlain on Wyoming State Geologic Survey (WGS) geologic maps (Ver Ploeg, A.J., and McLaughlin, 2009, 2010; Ver Ploeg, 2007, 2009). Red box outlines groundwater flow model boundary. Red and orange points show locations of geophysical logs and hydraulic head data. Area covered by each hydrogeophysical layer increases with depth from HL1 to HL4, respectively. a) Average resistivity of top layer, HL1, not included in groundwater model. b) Average resistivity of uppermost layer of groundwater model, HL2. c) Average resistivity of middle layer of groundwater model, HL3. d) Average resistivity of lowest layer of groundwater model, HL4.

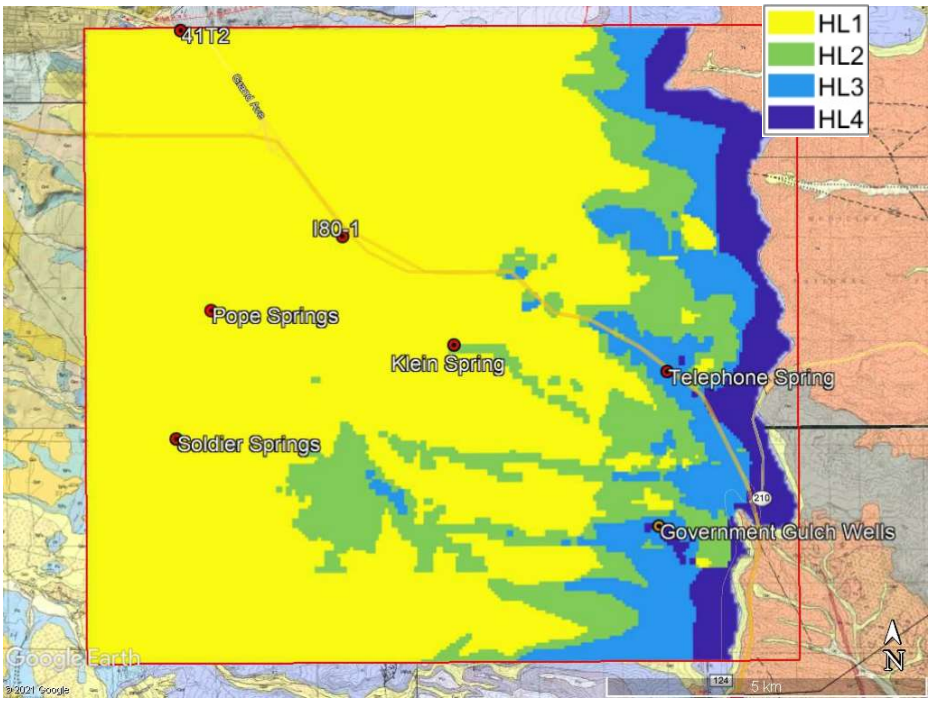

Figure 4.

Map view of extents of hydrogeophysical layers HL1 through HL4 overlain in Google Earth on WGS geologic maps. Groundwater model domain outlined in red, monitoring wells, pumping wells, and perennial springs shown in red and orange. HL1 is not incorporated into the groundwater model. However, the extent of HL1 defines where a much lower amount of recharge is assigned to the underlying grid cells.

Methods:

Airborne Electromagnetics

For information on the AEM data collection and processing/inversion, please see the interim report submitted in July 2020.

Airborne Magnetics

Aeromagnetic data was collected in tandem with the AEM data. Initial processing was completed by the data acquisition contractor, AquaGeoFrameworks (AGF) as discussed in (Carr & Smith, 2020). The residual magnetic field aeromagnetic data is plotted in GeoSoft Oasis Montaj and exported to Google Earth. Magnetic susceptibility measurements of basement rock and mafic intrusions within the Laramie Range are taken using a ZH instruments SM30 handheld magnetic susceptibility meter. These measured susceptibilities vary many orders of magnitude, indicating basement rock type varies through the survey area. GeoSoft Oasis Montaj extension GYM-SYS is used to forward model the magnetic response along transects of the aeromagnetic data perpendicular to the anomalies using values on the same magnitude of the measured magnetic susceptibilities.

Borehole Geophysical Logs

The University of Wyoming, Wyoming Center for Environmental Hydrology and Geophysics as well as the University of Wyoming Near-Surface Instrument Center acquired borehole geophysical logs between 2015 and 2020 in monitoring wells within and near the survey area. Logs are taken in the JRA-1 well 4.2 km north of the survey area just west of the edge of the Satanka contact, in the 41T3 well 45 m east of JRA-1, in the 41T2 well 2.5 km north of the western edge of the survey area, and in the Government Gulch well in the SE section of the survey area (Figure 1). Wells JRA-1, 41T3, and 41T2 penetrate a substantial portion of the Casper Formation, whereas logs from Government Gulch (GG) penetrate the lower Alpha of the Casper Formation, the Fountain formation, and end in the underlying Sherman Granite and a Ferromonzonite rich member of the Sherman granite. The combination of all wells into one file gives lithologic and geophysical data spanning the Casper, Fountain, and underlying basement formations.

GeoScene3D Modeling

AEM data, borehole geophysical logs from monitoring wells within and near the survey area, and well logs from the State Engineers Office (SEO) website are imported into GeoScene3D. Electromagnetically significant layers are picked to train the smart interpretation algorithm, which then picked these layers throughout the AEM data. These layers are then extensively fine-tuned to best represent areas where the algorithm had trouble due to low contrast in resistivity between hydrogeophysical layers in the AEM data, often in areas where layers "pinch out". Where model layers disappeared due to outcropping, these layers are run through the "grid adjustment" utility to assign elevations less than the overlying layer or topography to make sure each layer exists at all points within the AEM domain (*GeoScene3D Builder*, 2021). This is necessary for translating the layers from the AEM data into a groundwater flow model. Views looking at the model from each corner in GeoScene3D shown in Appendix 1, Figures 1 - 4.

MATLAB

MathWorks MATLAB is used extensively to create figures of the AEM data (*MATLAB: R2021a*, 2021). After GeoScene3D layers are finalized, the layers are exported as text files on a 50 m UTM grid. Each layer has an elevation at each grid point, creating a 3D model of the hydrogeophysical layers in the AEM data. Using these layers, AEM resistivities are averaged for each layer, allowing average resistivities to be plotted for the entire survey area where each layer exists. Map view of the hydrogeophysically significant resistivity layers, HL1 through HL4, shown in Figure 3.

Groundwater Modeling

This section details the conversion from the hydrogeophysical layers picked in GeoScene3D to a groundwater model. USGS MODFLOW 6 is used to model the saturated groundwater flow within the Casper and Fountain Formations, and USGS MODPATH 7 is used to plot particle path lines within the system. The USGS python interface, FloPy, is used to create source files for both the MODFLOW and MODPATH executable. This python interface makes it easy to alter model input variables, allowing for quicker adjustments of all model parameters to best fit the model to historic hydraulic head data (Bakker et al., 2021).

1. Model Layers

Layers from GeoScene3D are exported into MATLAB, where the cubic spline method in the function griddedInterpolant() is used to interpolate the elevation of each layer from the edges of the AEM data to a larger grid with 199 cells per row and 223 cells per column (*MATLAB: R2021a*, 2021). Corner elevations for the larger grid are estimated to constrain the

extrapolation of each layer. The edges of this grid are picked sufficiently outside of the area of interest to ensure boundary conditions do not influence the flow direction between Pope and Soldier Springs and the Interstate 80 corridor. This groundwater model incorporates the three major saturated hydrogeophysical layers seen in the AEM data. Layers in the groundwater model are referred to as HL2, HL3, and HL4, where HL2 is the top layer and HL4 is the bottom (Figure 2). The top layer, HL1 is not incorporated into the groundwater flow model since it is assumed to be the resistive, unsaturated layer overlying the groundwater flow model. View of layer elevations before and after extrapolation to groundwater model grid shown in Figures 1 and 2 of Appendix 2.

USGS MODFLOW 6 requires that all layers exist everywhere within the model domain (Hughes, Langevin, & Banta, 2017; Langevin et al., 2017, 2021). To appropriately address areas where model layers "pinch out," grid cells can be turned on, off, or can act as vertical pass through cells through the model discretization package, "idomain" assignment (Bakker et al., 2021). Grid cells to the east of the Casper – Basement contact are assigned idomain values of 0, which creates a no flow boundary along the eastern edge of the groundwater model. Cells within the upper two layers that pinch out are assigned idomain values of -1, which allows water within the model to pass through to the lower most active layer from recharge. All other grid cells are assigned idomain values of 1, indicating they are "turned on" in the model.

To account for multiple layers of the aquifer system, "iconvert" values within the storage package is assigned for each cell in the model. Cells which are the uppermost "on" cells are assigned values of 1, which indicates they are to be treated as unconfined cells. All other "on" cells are assigned values of 0, which tells the model to treat these cells as confined. If the uppermost cells' hydraulic head values become larger than the upper elevation of that layer, the cell is treated as a confined cell.

2. Model Hydraulic Properties

Boundary conditions are chosen to best replicate real-world conditions. Since there exists no groundwater divides on the west, north, and south boundaries, each of the grid cells along these model edges was assigned a constant head value. The east boundary is assigned a no flow boundary following the lithologic contact between the Casper Formation and Basement outcrop. The base of the model is a no flow boundary.

Starting model water level data is adapted from the 2005 potentiometric surface map using the scatteredInterpolant() function's "natural" interpolation method in MATLAB (*MATLAB: R2021a*, 2021; Taboga, 2005). Since water levels from this data did not all include depth to the screen of each well, it is unclear from which HL2 - HL4 layer the water level data came from. Additionally, there exists very little hydraulic head data for more elevated sections of the model, which

corresponds to the HL4 layer of the groundwater model. Because of this lack of data, starting hydraulic head values are assigned to be the same for each layer of the model.

Hydraulic conductivity values are assigned to every grid cell within the model based on average layer AEM resistivities in each cell. Using the range of hydraulic conductivity (K) values from bulk depths in the borehole NMR data and comparing them to pump test K values in the Casper Aquifer Protection Plan, each grid cell is assigned a horizontal K based on ranges: resistivity below 325 Ωm = 3.55 ft/day, resistivity between 325 Ωm and 600 Ωm = 0.56 ft/day, and resistivity above 600 Ωm = 0.1 ft/day (Figure 5. Major faults in the model domain are assigned very low horizontal hydraulic conductivities in layer HL2 – 4 shown in Figure 5.b - 5d and Figure 6. as: red = 0.009 ft/day; orange = 0.02 ft/day; yellow = 0.03 ft/day. All these faults act as barriers to groundwater flow within each layer, however these faults do not change the assigned vertical hydraulic conductivities, meaning in some of the fault assigned grid cells water can move vertically more easily than horizontally. Aside from the fault systems, the overall Casper formation is an anisotropic system, thus vertical hydraulic conductivities generally are much lower than horizontal. A vertical hydraulic conductivity grid is created to account for flow between HL1 and HL2, and HL2 and HL3 by assigning areas within HL2 with resistivity below 325 Ωm = 0.15 ft/day, resistivity between 325 Ωm and 600 Ωm = 0.1 ft/day, and resistivity above 600 Ωm = 0.05 ft/day (Figure 5.a). Grid K values beyond the edges of AEM data are extrapolated to follow the general trend of each layer. This method is only used for the hydrogeophysical layers that are fully saturated (HL2 – HL4).

3. Water Balance

Precipitation data from PRISM, a 30-year average of monthly rainfall and snowmelt on a global 800 m grid, is used to estimate recharge to the system (*PRISM Gridded Climate Data*, 2004). Each groundwater flow model grid cell is assigned the nearest neighbor average precipitation from the PRISM model in MATLAB so each uppermost grid cell in the model has an assigned average monthly precipitation (*MATLAB: R2021a*, 2021). These values are then converted into feet per day. Precipitation values for each grid cell is divided by 2.3 to help account for evapotranspiration. Each row of grid cells that are overlain by layer HL1, are additionally divided by a numerical array ranging from 20 at the western edge of the model, to 2 at the eastern edge of the model. This gradient is necessary to allow enough recharge along the eastern side of the model, while decreasing recharge to the western side of the model enough to keep hydraulic head levels low enough to replicate historic data. Figure 7 shows this gradient in HL1 in comparison with the original PRISM data.

The grid cell in layer HL2 closest to the Soldier Well house is assigned pumping rates for each stress period based on rates per month averaged over 10 years from data provided by the City of Laramie Water Resources Administrator, Darren Parkin. Locations of private wells from the SEO database in neighborhoods within the groundwater model domain are assigned daily

pumping rates based on Wyoming Water Development Office's average use per resident statistic, 505 gal/day ("E-Permit," n.d.; Office, n.d.).

4. Running the model

The groundwater model is assigned thirteen stress periods. The first period is steady state, with precipitation and well pumping rates that represent averages. This allows the model to calibrate itself. The following twelve stress periods each have four time steps representing a week each. The inputs to each stress period are based on the monthly averages for precipitation from the PRISM Climate Model, pumping at the Soldier Well, and average pumping rate per day per household in Wyoming (Wyoming Water Development Office; *PRISM Gridded Climate Data*, 2004).

Constant head boundaries, hydraulic conductivities, and precipitation values are methodically altered to create a groundwater flow model that more closely represents reality. The utility observation package is used to extract hydraulic head values for specific grid cells within the model to compare to historic hydraulic head data to model outputs for each stress period and time step (GG Casper Deep Well, I-80 Monitoring Well, Pope Springs Wells, and the elevation of two perennial springs: Klein Spring, and Telephone Canyon Spring). Once a model is created, replicating historic hydraulic head measurements, two more models are created with the same starting, recharge, and boundary conditions, but altering the low K faults and well pumping rates. The three final models created are as follows: (M1) with faults and pumping at Soldier Springs and household wells, (M2) with faults and no pumping at Soldier Springs or household wells, and (M3) with no faults or pumping to demonstrate how the low K faults acting as barriers to lateral groundwater flow are necessary to replicate hydraulic head levels at all points with known hydraulic heads within the model domain.

5. MODPATH – Estimating /Tracking Groundwater flow thru the model via predictive modeling software, MODPATH 7

Once M1 is calibrated to historic hydraulic head measurements, USGS MODPATH is used to track particle movement in model M1 to visualize how water moves through the aquifer, and understand where spills on the interstate might flow within the aquifer. In order to best create flow paths that visualize this flow, all stress periods in M1 are run as steady state. This is because when MODPATH is run with transient stress periods, the distance the particles track are not far enough to demonstrate movement within the entirety of aquifer. To run MODPATH 7, particles at specified points within the model are released during the first stress period. These particles are then "forward tracked" throughout each of the model stress periods. Forward tracking scenarios are created for M1 for particles released that are captured by the Soldier Springs well, and for particles released along the I-80 corridor.

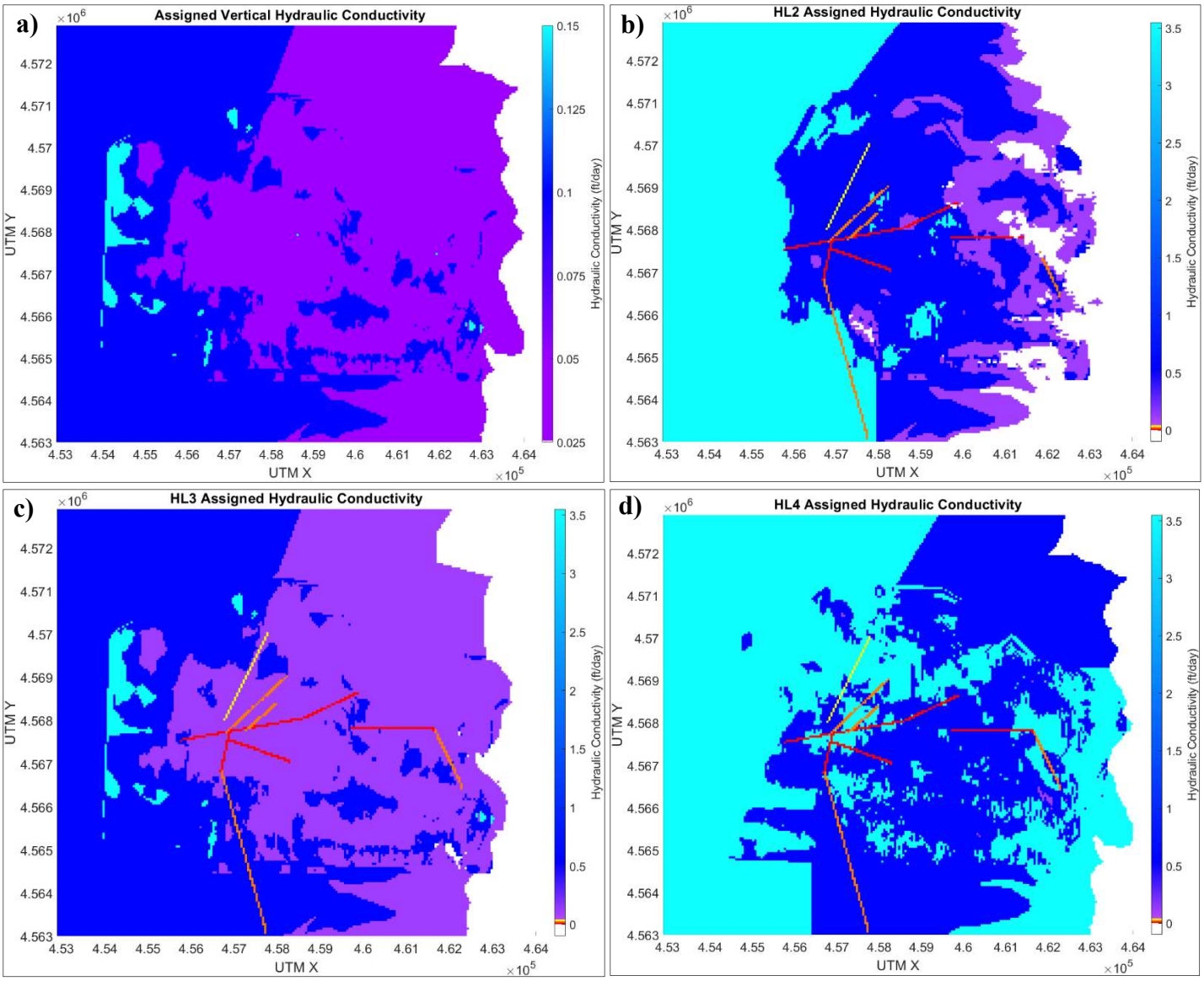

Figure 5.
Hydraulic conductivity arrays for vertical flow and model layers HL2 – HL4. Note the scale difference between a) and b) – d). a) K vertical: Cyan = 0.15 ft/day, Blue = 0.1 ft/day, and Purple = 0.05 ft/day b-d) K HL2 - HL4, respectively: Cyan = 3.55 ft/day, Blue = 0.56 ft/day, and Purple = 0.1 ft/day. Faults represented by: Yellow = 0.03 ft/day, Orange = 0.02 ft/day, and Red = 0.009 ft/day.

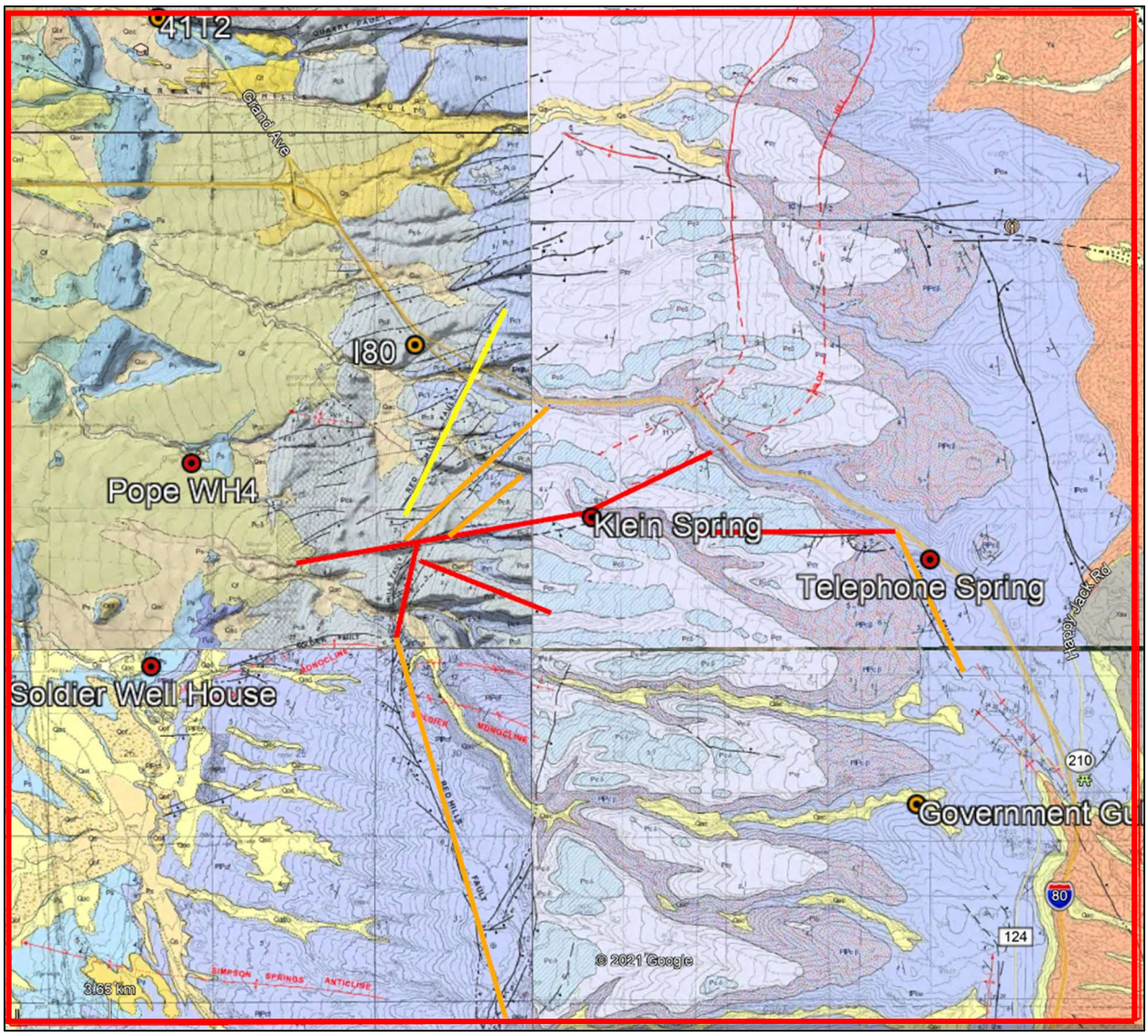

Figure 6.
WGS geologic map with groundwater model domain outlined in red, and major faults added into model shown in red, orange, and yellow maps (Ver Ploeg, A.J., and McLaughlin, 2009, 2010; Ver Ploeg, 2007, 2009). These faults have hydraulic conductivity values of 0.009 ft/day, 0.02 ft/day, and 0.03 ft/day, respectively. Pope Springs, I-80 Monitoring Wells, Klein Spring, Telephone Spring, and Government Gulch Monitoring Wells shown in red, and orange are locations where hydraulic head from the groundwater models are compared to historic data and ground surface elevation.

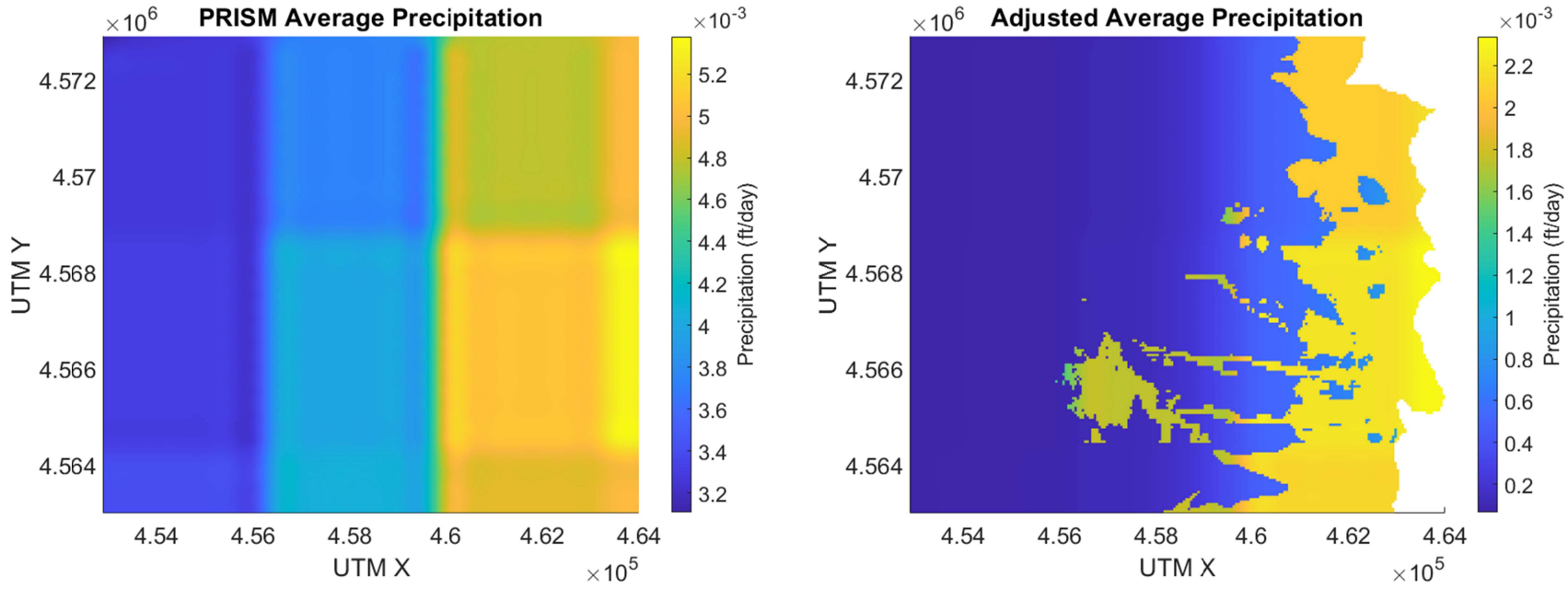

Figure 7.

a) PRISM Model average precipitation and b) final adjusted precipitation amounts added to the models. Note the scale difference between the two – there is much less precipitation that is directly added to the model than actually falls according to the PRISM model. This helps to account for evapotranspiration. Additionally, precipitation at the grid points where HL1 exists in the model domain are significantly decreased. This is necessary for the hydraulic head values to be high enough at Telephone Springs and Government Gulch, while low enough at the I-80 and Pope Springs Wells and at Klein Springs.

Results/Discussion:

Magnetic Field data

The aeromagnetic data informs our knowledge of the strength of Earth's magnetic field above a certain point on Earth. Measured changes in aeromagnetic data over an area indicates changes in the magnetic response of the underlying rock to Earth's magnetic field (Hubbard & Linde, 2011). The more iron rich a rock, the larger the magnetic anomaly. Magnetic susceptibility is a measurement of how much a rock can be magnetized by an external magnetic field (Borradaile, 1988). Since the sedimentary rocks that make up the Casper Aquifer do not have any significant magnetic susceptibility, the aeromagnetic data indicates how iron rich the basement rock is throughout the survey area.

Initially, it is assumed that the aeromagnetic data would show an increasing magnetic gradient from west to east as the weakly magnetic Sherman Granite rises to the surface at the summit of the mountain front. However, the data (corrected for diurnal drift and the International Geomagnetic Reference Field) show that there exist two significant anomalies disrupting that trend, one in the SE, the other a broad magnetic high that appears diagonally from SW to NE, shown in Figure 8. These surprisingly large variations in the residual magnetic field across the survey area indicate the presence of a different type of rock in the basement.

To investigate what rock types might be causing the large anomaly in aeromagnetic data, forward models were created using measured susceptibilities from local rock samples and outcrops. These values came both from the geophysical log of the Government Gulch monitoring well, and measurements of Sherman Granite and mafic diabase dikes in the Laramie Range (see Table 1). The forward models (see Figure 9.) suggest magnetic susceptibilities mafic diabase dikes account for the magnetic anomalies in the aeromagnetic data. While ferromonzonite has been located in the Government Gulch Monitoring well, the magnetic susceptibilities of these rocks are not large enough to account for the magnetic high in the SE of the survey area. Only magnetic susceptibilities of the same magnitude as the mafic diabase dikes in the Laramie Range can account for both the large high and low in the center and west of the survey area, and the smaller high in the SE of the survey area.

Intrusions in the crystalline basement can cause structural changes in the basement rock that indicate areas with increases in fracture density in overlying sedimentary layers. This consequence of basement mineralogic and structural changes is interpreted to create areas of increased hydraulic conductivity between HL2 and HL4. Figure 10. shows the residual magnetic anomaly overlain on both the depth to basement from the AEM data, and the mapped geologic structure. The magnetic highs caused by mafic diabase dikes are correlated to the surface mapped monoclines as well as changes in the surface slope of the basement rock. This is

especially noticeable in the northern part of the survey area where the Pilot Hill Monocline outlines the edges of the large magnetic high (Figure 10.a).

To quantify the hypothesis that decreased resistivity in HL3 reflects permeability pathways, Figure 10.b shows the average resistivity of HL3 projected onto the basement topography and WGS geologic maps. Areas where the basement slope changes can cause decreases in the overlying resistivity of HL3, whereas mapped faults at the surface correspond more to increases in resistivity. Examples of both are readily observed in Figure 10.b - the decrease in resistivity cause by basement structures is circled in box 1), and examples of faults causing increases in resistivity are circled by box 2). Both Figure 10. a) and b) suggest water movement between HL4 and HL2 is related to deep structure underlying the Casper Aquifer rather than fractures and faults that have been mapped at the surface.

Borehole Geophysical Logs

Borehole geophysical logs allow airborne geophysical data to be correlated to "ground-truthed" geophysical and hydrologic properties. Although these two types of measurements vary in scale, averaging sections of geophysical logs to compare to AEM data allows relationships to be made between AEM resistivities and hydrologic properties such as nuclear magnetic resonance (NMR) estimates of hydraulic conductivity (K). All boreholes except the Government Gulch well are outside the AEM survey grid. Yet, JRA-1, 41T2, and 41T3 are close and are assumed to be reasonable proxies for estimating physical and hydraulic properties within the AEM survey grid.

In Figure 11, depth of the formation sequence is shown on the far left, with member contacts shown to its right. EM resistivity is an electromagnetic induction measurement of how well current flows through the rock surrounding the borehole. The 64" Normal Resistivity is a direct current measurement of the rock's ability to conduct current. Gamma shows the amount of natural radiation of potassium (K), thorium (Th), and uranium (U) isotopes within the rock. Practically, the gamma response is used to infer the presence of clay minerals within the sedimentary rocks. For the crystalline basement, gamma mostly indicates relative abundance of K, Th, or U rich minerals. Magnetic susceptibility is a measurement of the degree to which a rock can be magnetized by an external magnetic field. Changes in the slope of the fluid temperature and fluid conductivity indicate groundwater inflow to the borehole. The Inflow/Outflow logs based on normalized Spinner Flowmeter logging indicate depths within the borehole where there is groundwater interaction between the borehole and surrounding formation. Finally, the NMR total porosity and free fluid shows porosity versus interconnected pore space with depth in the formation.

Comparing these geophysical logs to a few sample AEM soundings shows how the AEM data averages resistivities over large sections of rocks, while the borehole geophysical logs show a

more detailed image of the actual material properties of these aquifer rocks. These comparisons allow for the "ground-truthing" of the large scale AEM resistivity to hydrologic parameters. Comparing normal resistivity and NMR in the JRA-1 well shows high resistivity corresponds to low porosity and free fluid content and vice versa, seen as lines a and b respectively in Figure 11. This in addition to low clay content as shown by gamma in the JRA-1, 41T2, and 41T3 wells, indicates that areas of low resistivity in the AEM data likely correspond with higher permeability rather than clay content. Line c) highlights a depth with a sharp slope change in the fluid temperature and conductivity log data in 41T2 that corresponds with a spike in the Inflow/Outflow logs, which is an inferred large bedding plane fracture providing abundant groundwater flow, which supports the interpretation that there exist areas of high water movement within the aquifer. In box d, the Government Gulch magnetic susceptibility shows layers of higher susceptible rock overlying rock with more constant susceptibility. These changes in magnetic susceptibility are an additional ground truth to our understanding of the type of basement rock that underlies the Casper Formation.

Groundwater Modeling

1. Boundary and Starting Conditions

The PRISM average precipitation values were too large for the model to handle with reasonable K values in each layer, this is assumed to be due to evapotranspiration. To account for this, all grid cell daily precipitation values are decreased so that hydraulic head values given by the model closely mimic historic data. Additionally, through this process, it became clear that precipitation could not be significant in the lower elevation region of the model. To easily account for this, in areas where highly electrically resistive layer HL1 existed, recharge to the model was significantly decreased, working under the assumption that in these areas surface water had more unsaturated rock to flow through. Creating a lower precipitation layer through using where HL1 exists allowed hydraulic head values to be much more realistically replicated. This shows that recharge to the aquifer is coming mostly from the more elevated regions of the aquifer. Additionally, this implies that spills in the lower portion of the I-80 corridor are unlikely to penetrate to the water table and contaminate the municipal water source.

2. Structure, Resistivity, and Hydraulic Conductivity

As evident in Figure 6., there exist plenty of mapped structure within the groundwater model domain. When comparing these structure to the averaged AEM resistivities in each layer, there becomes trends between deep structure and resistivity as well as mapped faults and resistivity, both of which have ties to hydraulic conductivity. Figure 3. shows the average AEM resistivity for each layer HL1-HL4 overlain on the WGS geologic map. As previously stated, in areas where

there exist deep structure, there are correlated decreases in resistivity in the overlying layers (see Figure 10. These decreases in resistivity are transformed into areas with the highest assigned hydraulic conductivity in both layers HL2 and HL4, and a higher value in HL3. Since the vertical hydraulic conductivity is based on HL3, this additionally leads to higher vertical hydraulic conductivities in the groundwater model. However, areas where there are more densely mapped surface faults in the geologic maps are correlated to areas with higher AEM resistivities. These are sometimes located along the faults which were added as barriers to horizontal flow in the groundwater model. Lower K values were assigned to these grid cells, indicating that in some areas water might preferentially move vertically rather than horizontally since the vertical hydraulic conductivity is higher. These structural elements, especially the faults, are essential for replicating the historic hydraulic head measurements in the groundwater flow model.

3. Wells and Faults

Three models were created for this report to represent different pumping scenarios and show the importance of faults acting as barriers to lateral flow along the layers. Model One (M1) has both faults acting as barriers to flow and pumping at Soldier Springs, Model Two (M2) has low K faults but no pumping, and Model Three (M3) has neither faults nor pumping. Figure 12. - 16 show the water levels in each of the hydraulic head measurement locations in the survey area. In all five figures, it is clear that pumping at private wells and at Soldier Springs causes a slight decrease in water level at all locations (M2 vs M1), however, this decrease is small at only a foot or two.

The larger discrepancy between models is caused by the addition of low K faults into the model. Figure 12.-16 b) show that not including low K faults in the model causes inaccuracy in all five hydraulic head data points. This is especially important when considering the I-80 and Pope Springs hydraulic head values – both are higher than they should be, which would result in inaccurate predictions of groundwater flow direction. Figure 17. – 19 show the contour of hydraulic head, every 100 ft in M1 – M3, respectively. The faults added into M1 and M2 are very evident when looking at these contour plots, with an extension of the Pilot Hill Monocline Fault very visible in the middle, running east-west. M3 (Figure 19.) shows far less variability in the contours, with inaccuracy in the head levels along where the faults are included in the other models. This is important in improving our understanding of how water moves through the mountain front of the Casper Aquifer.

4. Particle Tracking

Figures 20 - 21 show particle tracking in M1. Tracking how particles flow in the groundwater model M1 is important for our understanding of the vulnerability of both privately owned wells as well as the Soldier well field. That said, constant head values assigned as boundary

conditions in the model create inaccurate effects near the edges of the model. These are not representative of how water is actually flowing in that region of the aquifer. Particle tracking lines close to the southern part of the model in Figure 20., and directions of tracking lines in the northwest corner of the model in Figure 21. should be ignored for the purposes of this discussion. Figure 20. is significant because it shows from where in the model the Soldier Springs well draws its source of water. The path lines in this figure intersect Pope Springs, as has been seen in the drawdown at Pope Springs when Soldier Springs is pumped. However, none of these flow path lines intersect the Interstate 80 corridor. This suggests that at the current rate of pumping (or less), that should spills on the interstate reach the water table the contaminant would not reach the cone of depression created by pumping at Soldier Springs. To further show that the Soldier Springs wells do not pull water from the interstate, Figure 21. shows path lines of particles released in the uppermost “on” layer of the interstate corridor. Tracking these particles shows that they flow mostly west, which creates little possibility for Soldier Springs to pump a contaminant, but causes a hazard to all the private wells that exist in that pathway, shown as black dots in both Figure 20. and Figure 21.

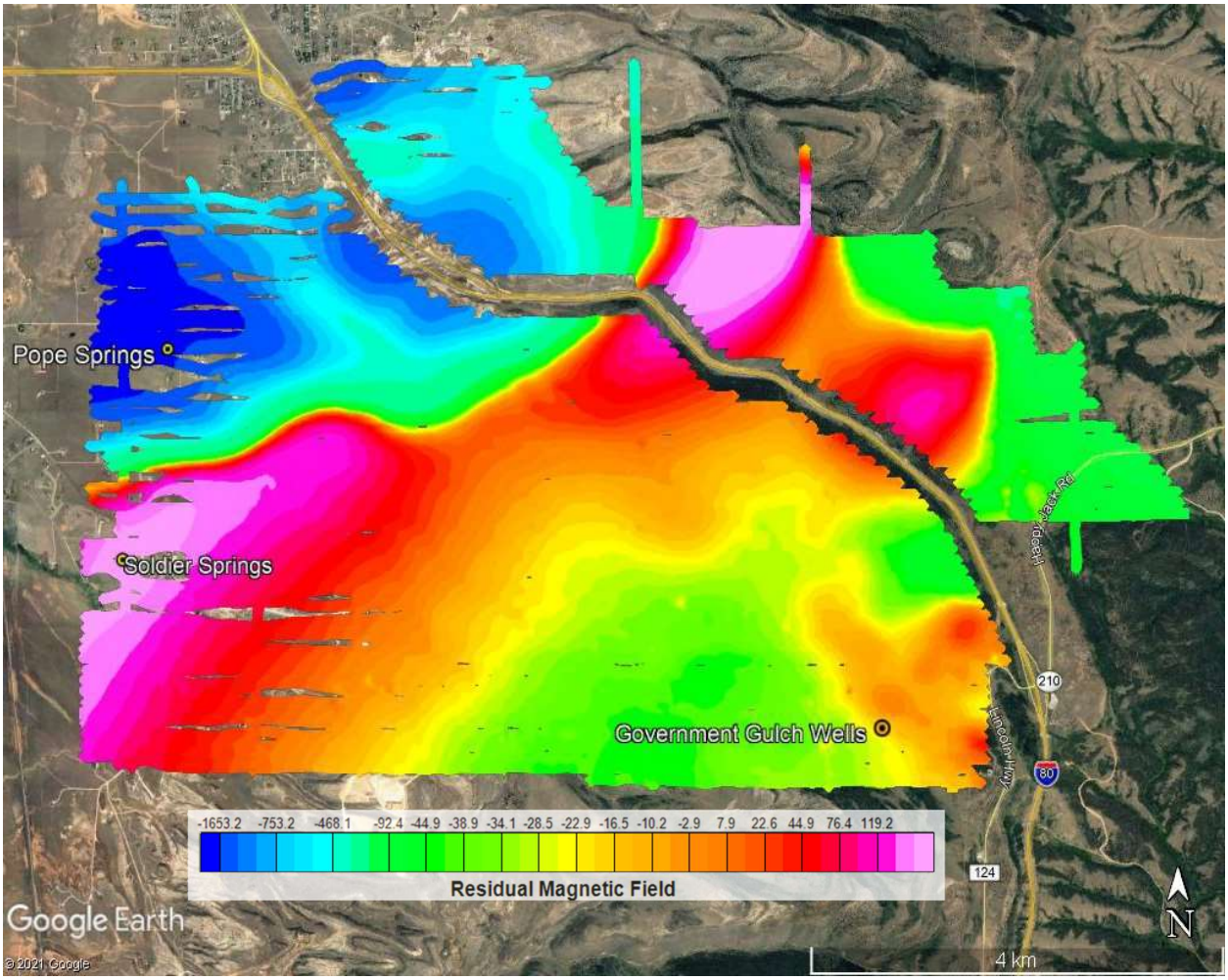

Figure 8.
Diurnal and IGRF corrected residual magnetic field (nT). If the basement were just Sherman Granite rising to the surface at the summit of the front slope, a smooth gradient would be expected. The magnetic high seen from the SW to NE of the survey area indicates mafic diabase intrusions into the basement. Highs in the SE of the survey area are ferromonzonite intrusions mapped by I-80 and seen in the government gulch monitoring well borehole geophysical log.

Site #	Geographic Coordinates (decimal degrees within 5 m)	Average of 4 Magnetic Susceptibility Measurements (10^-3 SI)
1	41.197582, -105.412411	104.17
2	41.197794, -105.412560	100.57
3	41.197934, -105.412590	100.48
4	41.198863, -105.413093	96.88
5	41.199179, -105.413247	108.15

Table 1.
Magnetic susceptibility measurements from the mafic diabase dike outcrop in the Laramie Range. These measurements are within the same magnitude as the values used to forward model profiles of the aeromagnetic data.

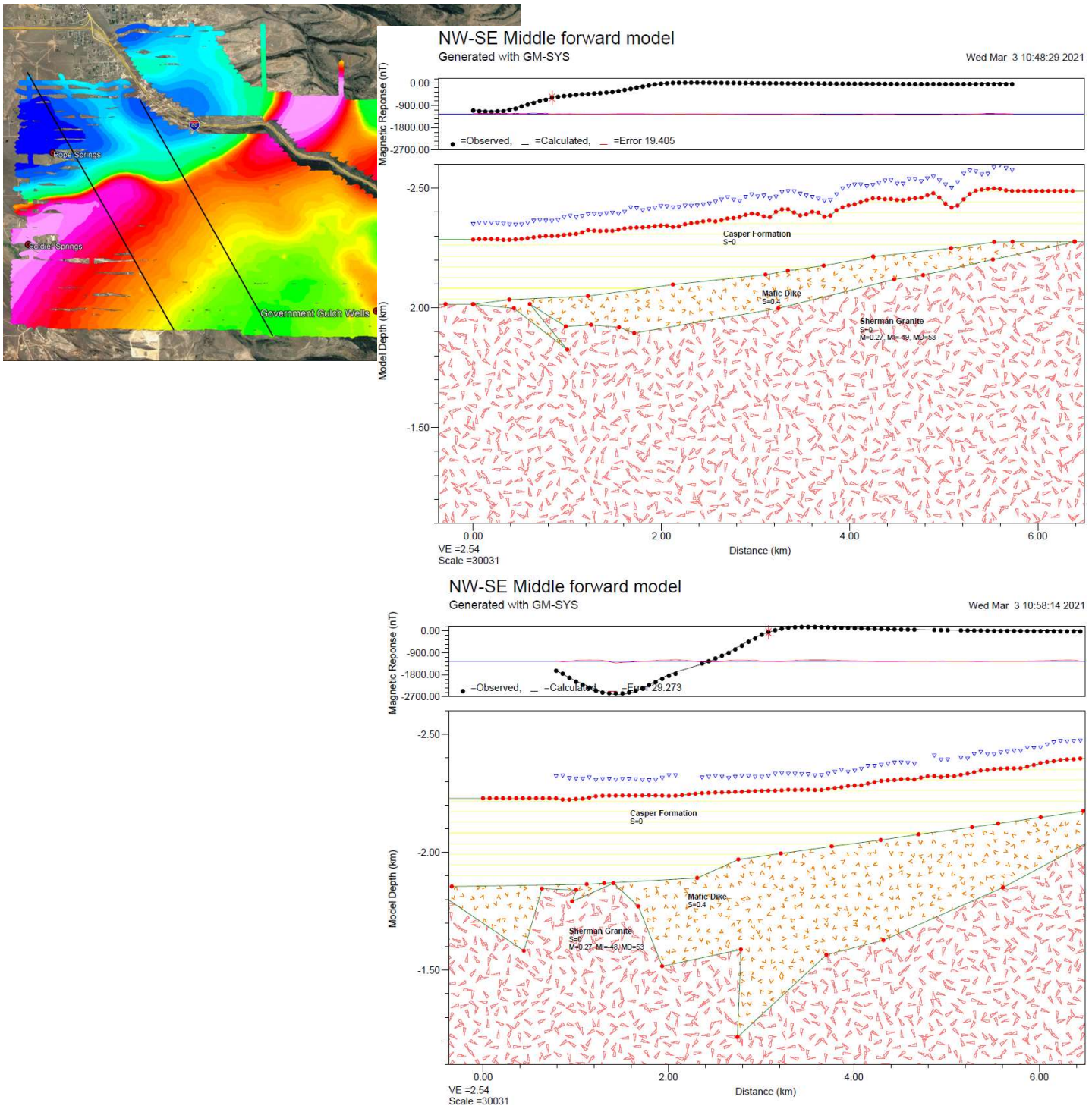

Figure 9.

Forward models of aeromagnetic data using measured magnetic susceptibilities from outcropping basement rock in Laramie Range and geophysical log from the GG well. The size and depth of the modeled mafic diabase dike accounts for the difference between the large and medium magnetic high along each profile.

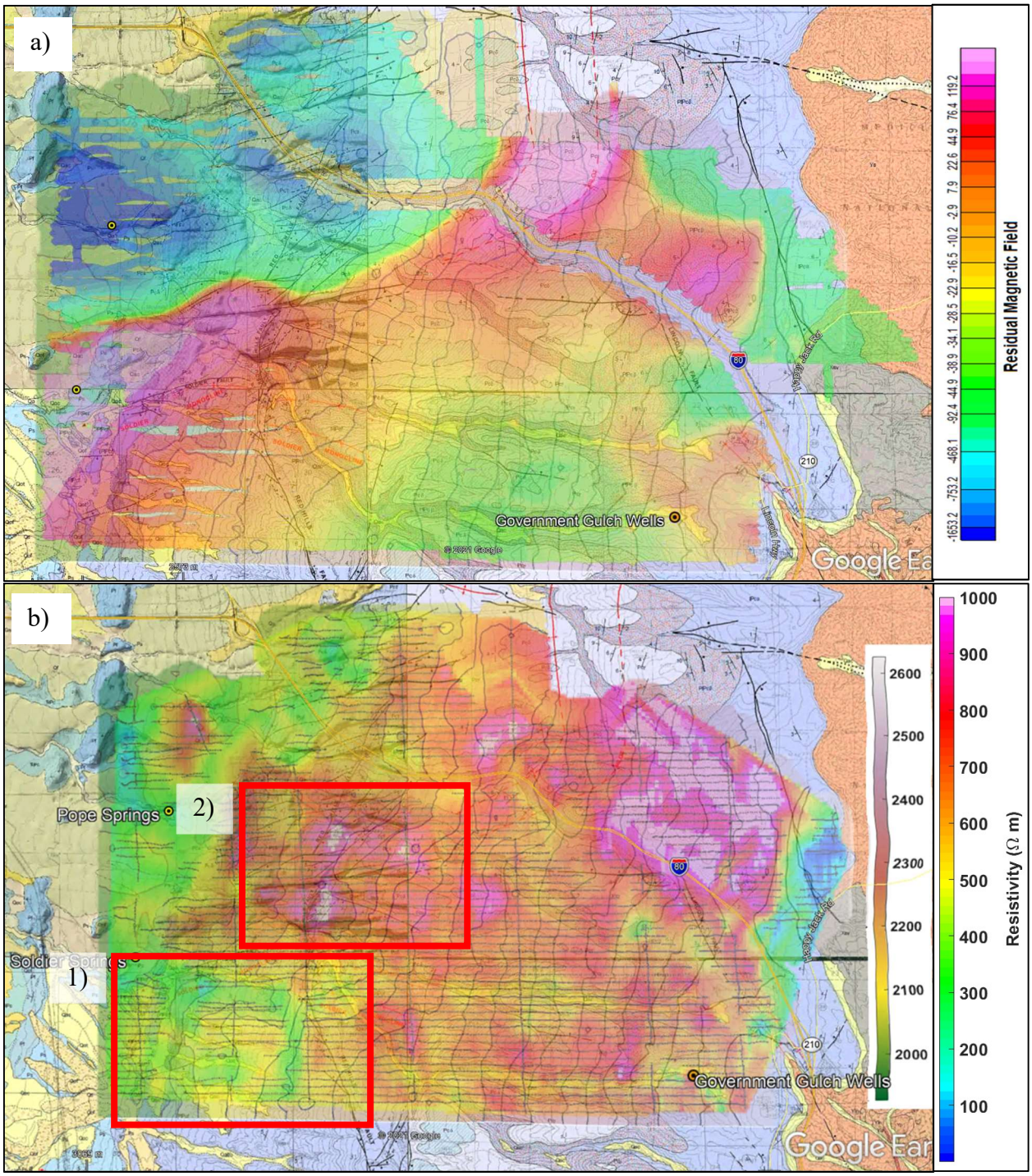

Figure 10.

Comparison between USGS geologic maps and airborne geophysical data (Ver Ploeg, A.J., and McLaughlin, 2009, 2010; Ver Ploeg, 2007, 2009) a) Residual magnetic field overlain on basement topography from AEM data and WGS geologic maps. b) AEM layer c average resistivity overlaid on basement topography from AEM data and USGS geologic maps. The red box in the bottom left is an example of an area where changes in the slope of the basement influences the AEM resistivity in the overlying hydrogeophysical layer.

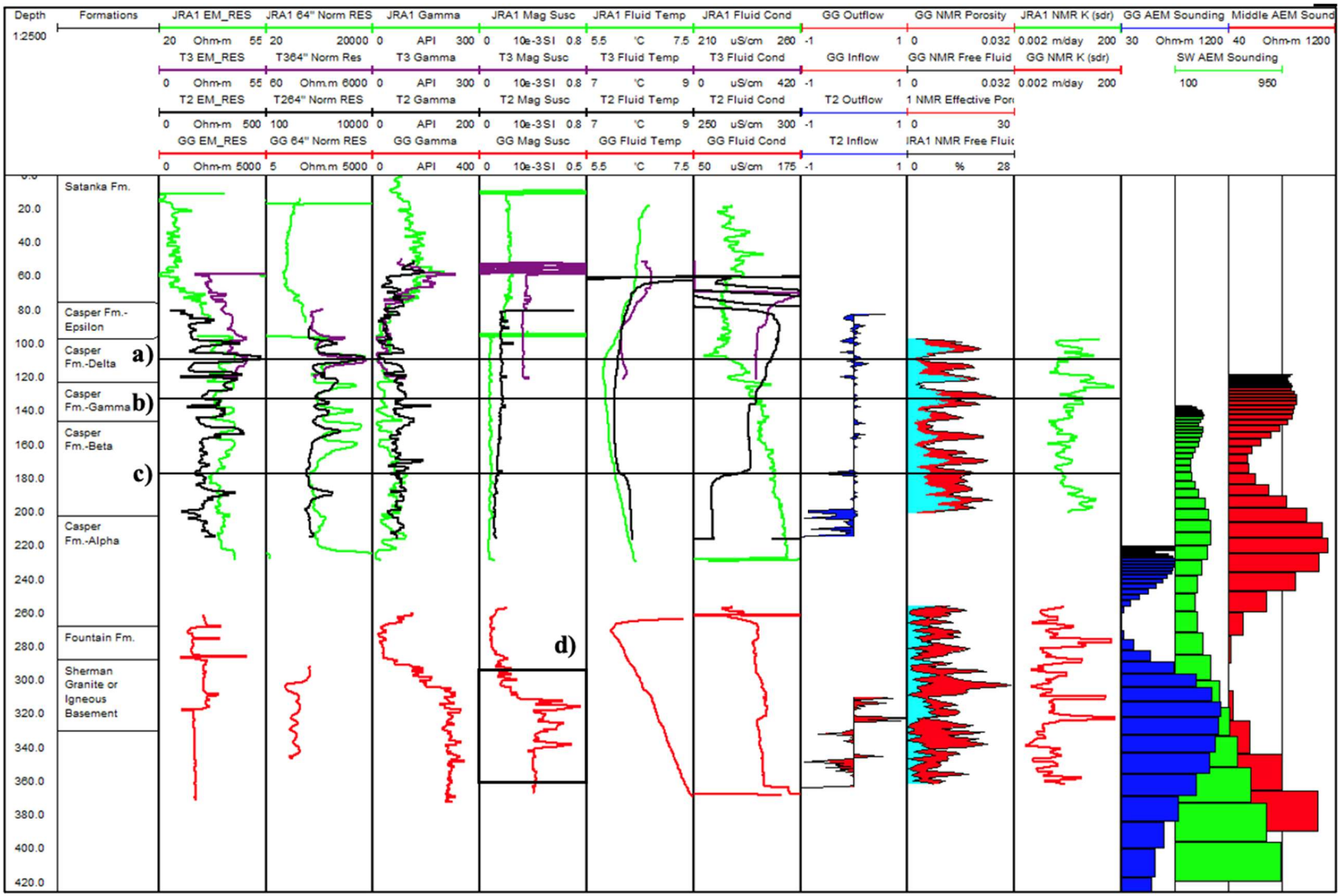

Figure 11. Geophysical logs from the JRA-1, 41T3, 41T2, and Government Gulch Monitoring Wells with example AEM soundings at approximate depths for comparison. Depth of each well approximated to each other based on depth to limestones and total formation depth in order to estimate geophysical measurements for entire Casper Formation, Fountain Formation, and crystalline basement sequence. From left to right, depth in meters, approximate boundary of Casper Formation sections, EM resistivity, 64 inch Normal Resistivity, Gamma, Magnetic Susceptibility, Fluid Temperature, Fluid Conductivity, Inflow/Outflow diagram, NMR Porosity and Free Fluid Content, NMR (sdr) hydraulic conductivity (K) calculation, and three example AEM soundings. Line a) represents where high resistivity corresponds to low porosity, and line b) shows the opposite relationship, both in the JRA 1 well. Line c) shows slope changes in the temperature and fluid conductivity in the T2 well correlates to a spike in the inflow/outflow diagram – likely a bedding plane fracture. Box d) circles changes in the magnetic susceptibility in the basement rock, showing more than one type of rock exists in the basement underlying the Casper and Fountain formations.

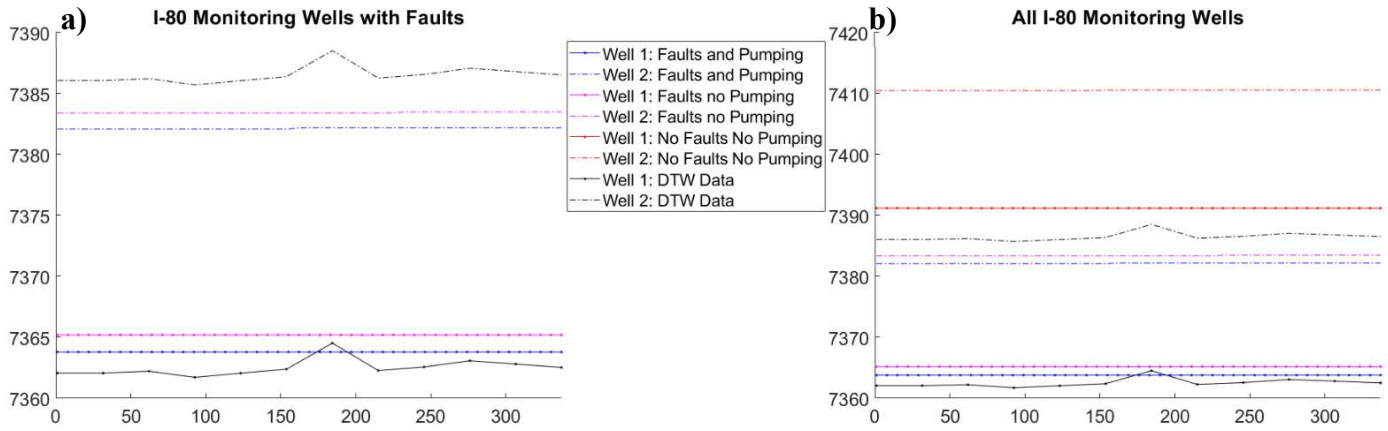

Figure 12.
Comparison between models and historic water level data for I-80 monitoring wells. Blue lines represent M1 with both faults added and pumping at Soldier Springs, pink lines represent M2 with added faults but no pumping at Soldier Springs, and red lines represent M3 with no faults and same starting and boundary conditions as M1 and M2. a) Historic water levels in the I-80 monitoring wells and water levels in the nearest grid cell within M1 and M2. b) Shows model with no faults in addition to the same data shown in a. Added faults have a large effect on the model ability to replicate these wells' hydraulic head data.

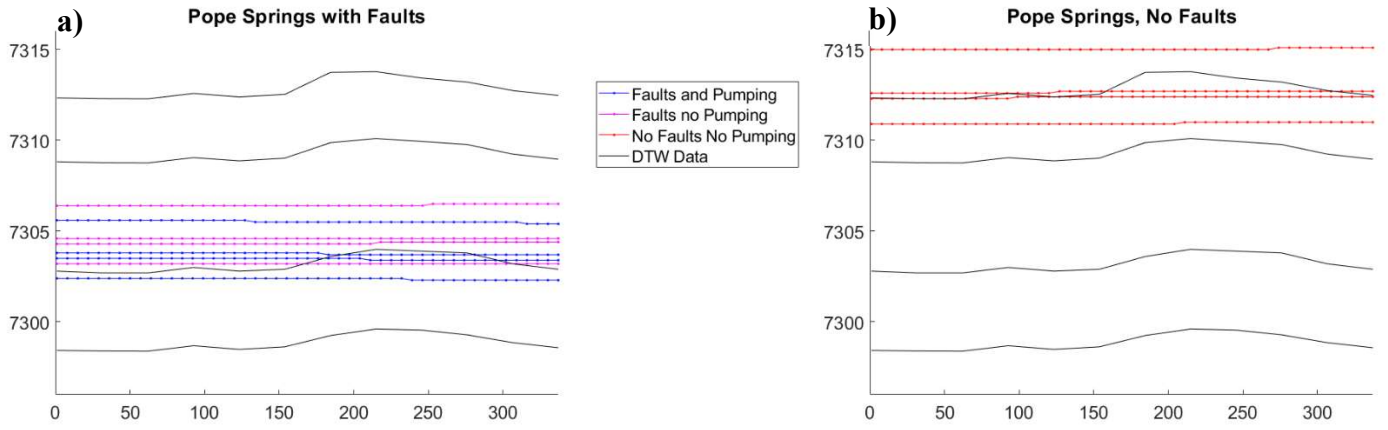

Figure 13.
Comparison between models and historic water level data for Pope Springs. Blue lines represent M1 with both faults added and pumping at Soldier Springs, pink lines represent M2 with added faults but no pumping at Soldier Springs, and red lines represent M3 with no faults and same starting and boundary conditions as M1 and M2. a) Pope Springs water level data shown in black, with the four nearest grid cells in M1 and M2 shown

in blue and pink. These values lie within the expected water levels. b) M3, no faults. The faults effect the modeling ability to replicated hydraulic head.

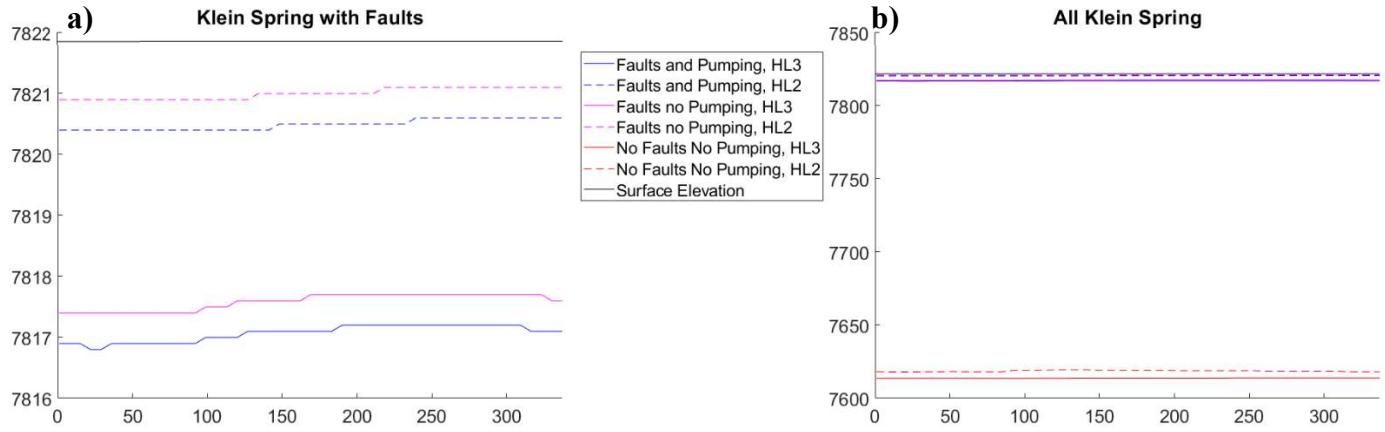

Figure 14.
Comparison between models and historic water level data at Klein spring. Blue lines represent M1 with both faults added and pumping at Soldier Springs, pink lines represent M2 with added faults but no pumping at Soldier Springs, and red lines represent M3 with no faults and same starting and boundary conditions as M1 and M2. a) Land surface elevation data shown in black, with M1 and M2 shown in blue and pink. Values from models one and two, layer HL2, are within two feet of the land elevation. b) M3, no faults. The faults drastically affect the model.

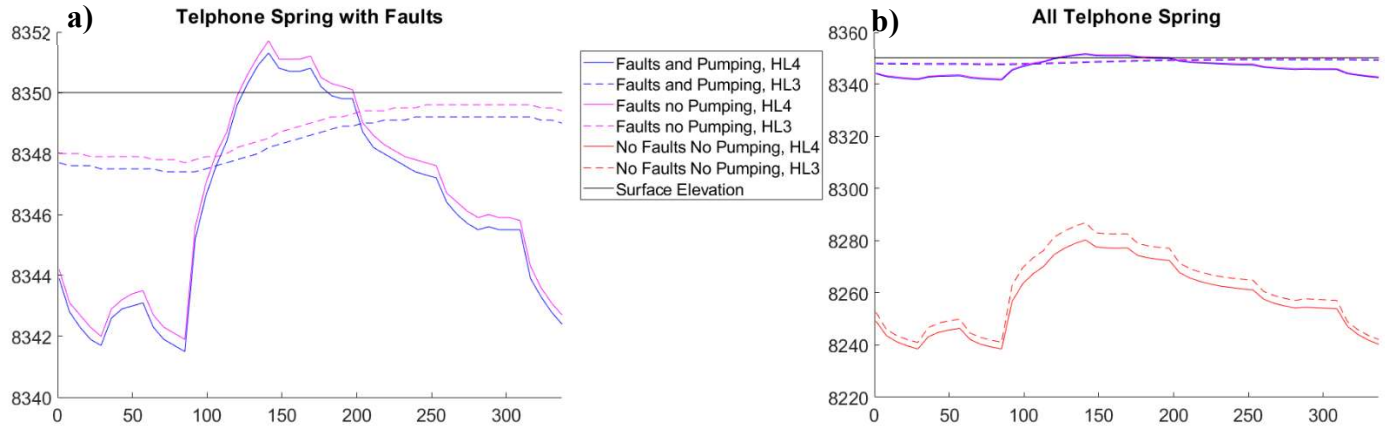

Figure 15.
Comparison between models and historic water level data at Telephone Springs. Blue lines represent M1 with both faults added and pumping at Soldier Springs, pink lines represent M2 with added faults but no pumping at Soldier Springs, and red lines represent M3 with no faults and same starting and boundary conditions as M1 and M2. a) Land surface elevation data shown in black, with M1 and M2 shown in blue and pink. Values from

models one and two, layer HL3, go above land surface during periods of high recharge in the spring. b) M3, no faults. The faults drastically raise the DTW at telephone springs.

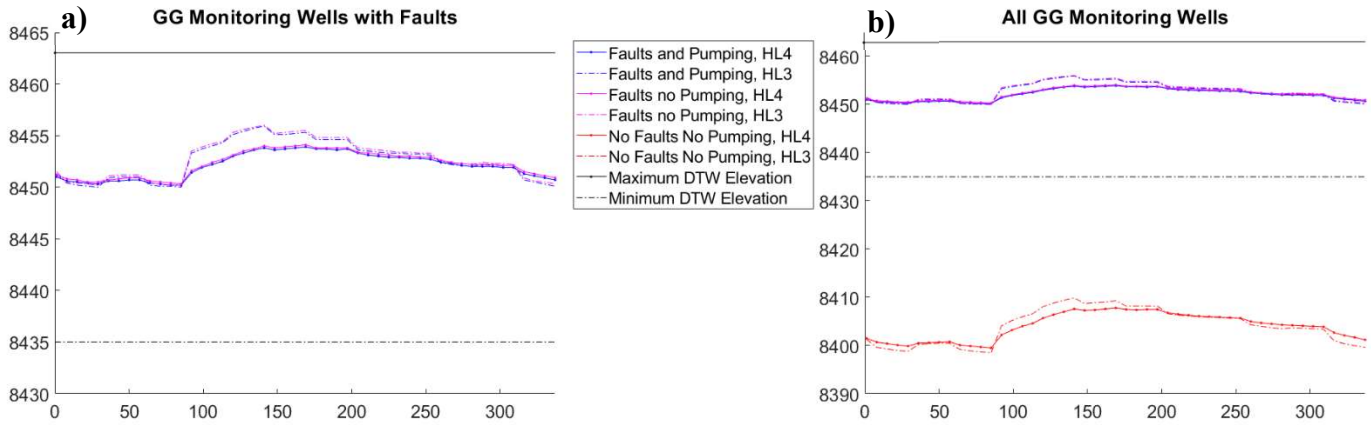

Figure 16.

Comparison between models and minimum and maximum water level at the Government Gulch (GG) monitoring wells and modeled values. Blue lines represent M1 with both faults added and pumping at Soldier Springs, pink lines represent M2 added faults but no pumping at Soldier Springs, and red lines represent M3 with no faults and same starting and boundary conditions as M1 and M2. a) Historic water levels in the GG monitoring wells and water levels in the nearest grid cell within M1 and M2. These values do not vary as much as water level data shows, but boundary conditions could be affecting the variability. The modeled values still fall within the expected range. b) Shows model with no faults in addition to the same data shown in a. Added faults have a large effect on the model ability to replicate these wells' hydraulic head data, causing the model to output values 50 ft lower than the models with faults.

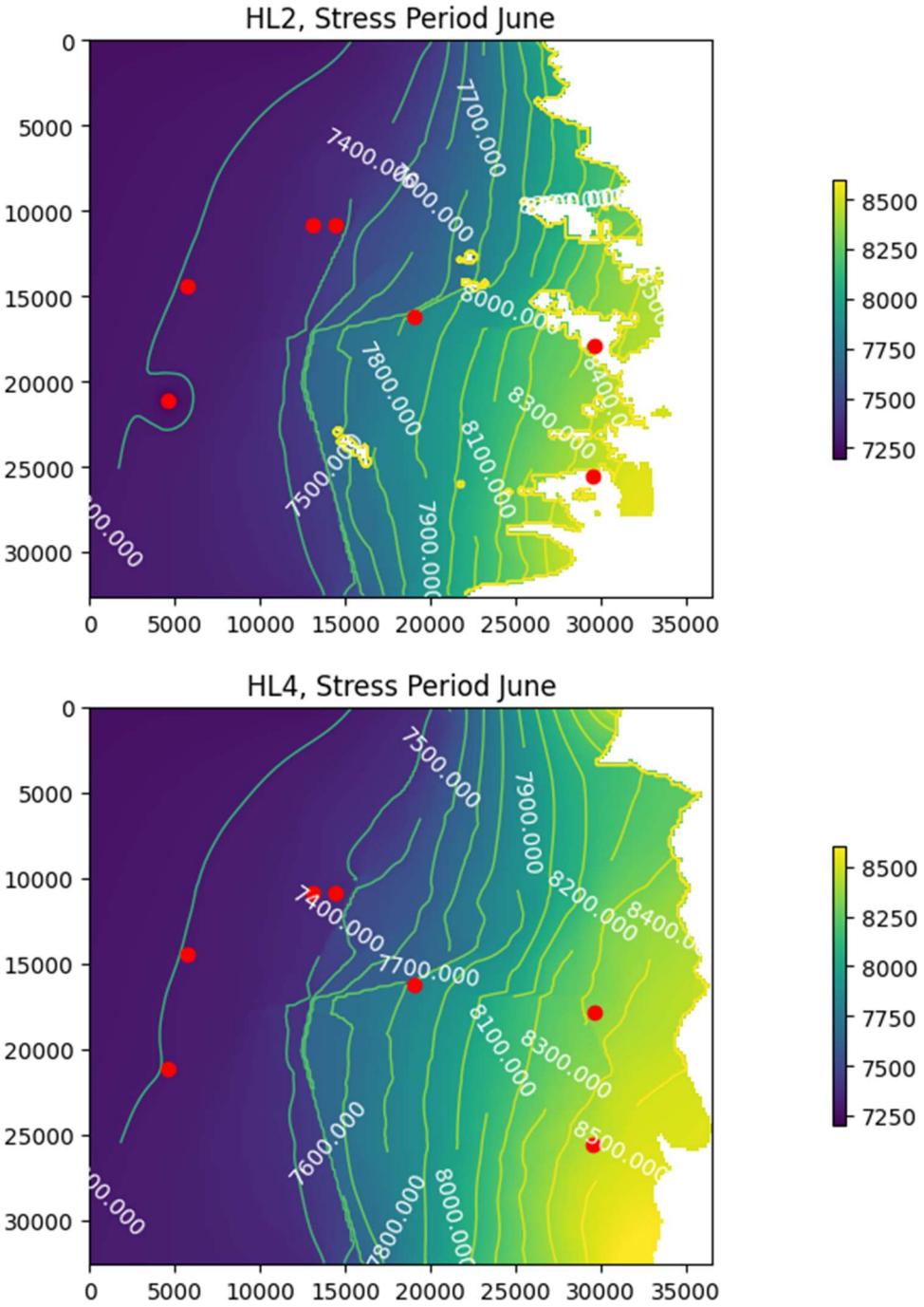

Figure 17.
M1 (low K faults and pumping) hydraulic head of June stress period. Soldier Springs, Pope Springs, I-80 monitoring wells, Klein Spring, Telephone Spring, and Government Gulch monitoring well signified by red dots. Low K faults acting as barriers to flow are evident by the sharp changes of direction in contours. Soldier Springs pumping effect on contours most evident in HL2.

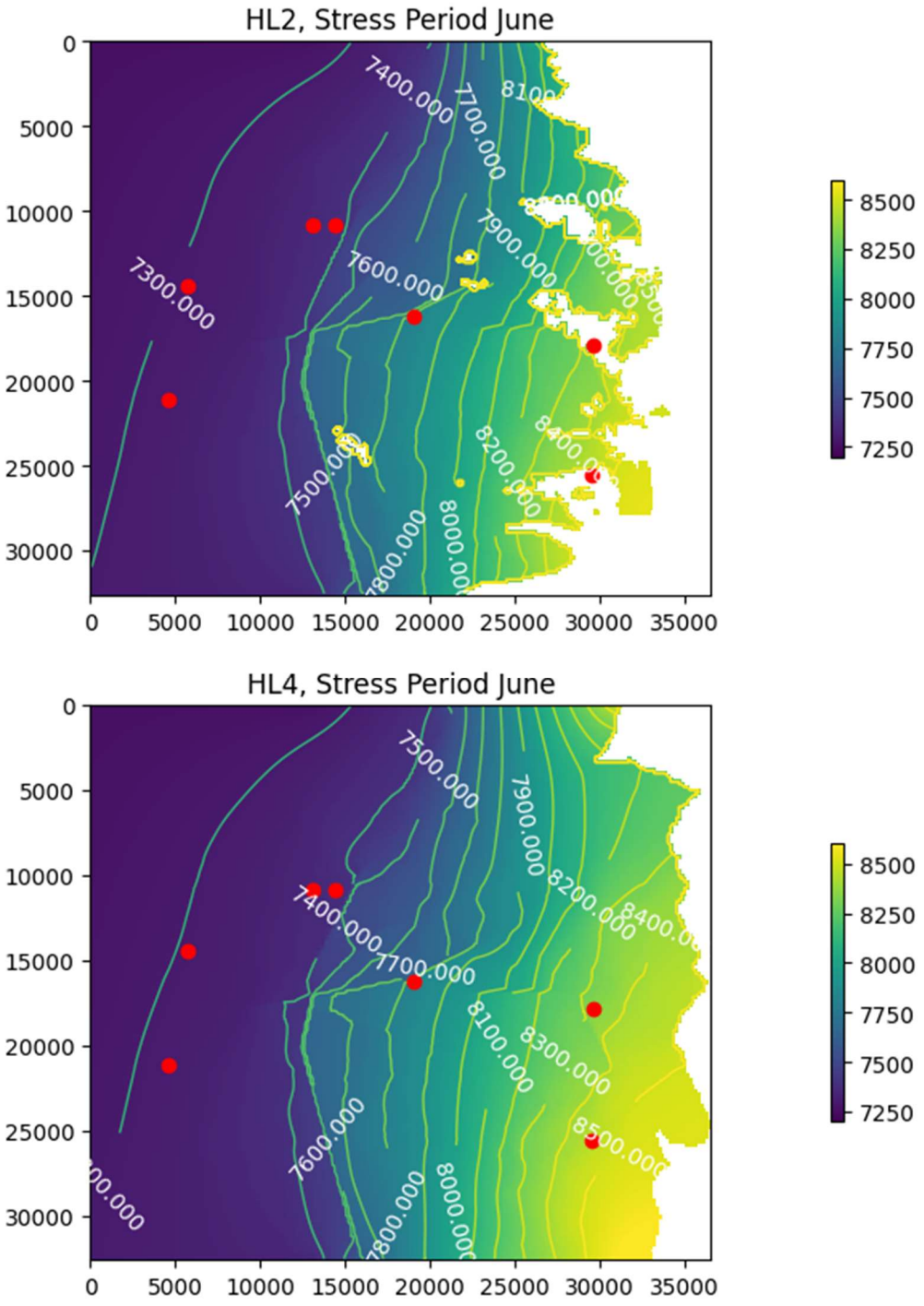

Figure 18.
M2 (low K faults and no pumping) hydraulic head of June stress period. Soldier Springs, Pope Springs, I-80 monitoring wells, Klein Spring, Telephone Spring, and Government Gulch monitoring well signified by red dots. Low K faults acting as barriers to flow are evident by the sharp changes of direction in contours.

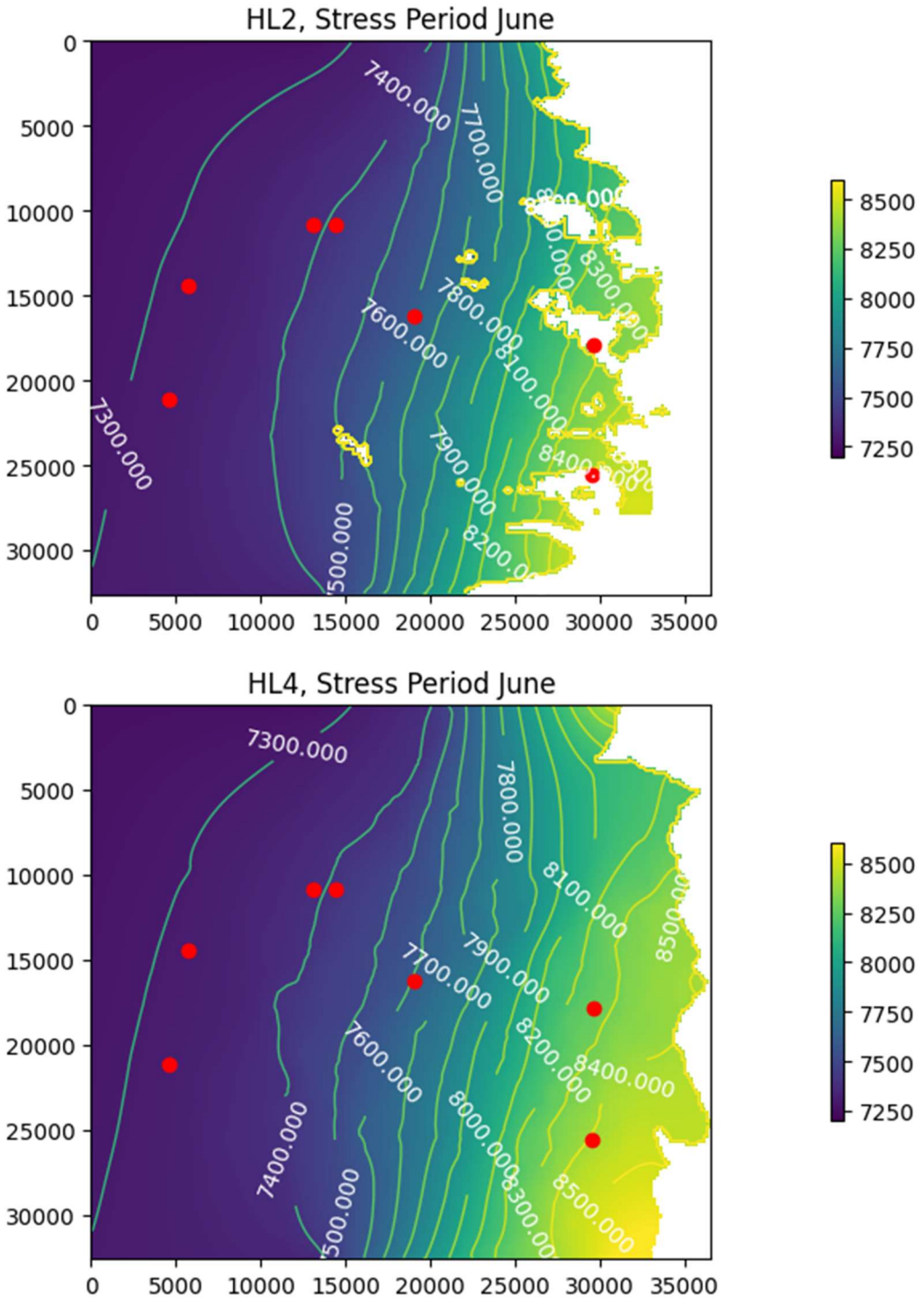

Figure 19.
M3 (no low K faults and no pumping) hydraulic head of June stress period. Soldier Springs, Pope Springs, I-80 monitoring wells, Klein Spring, Telephone Spring, and Government Gulch monitoring well signified by red dots. There are no longer sharp changes in direction of contours due to lack of low K faults.

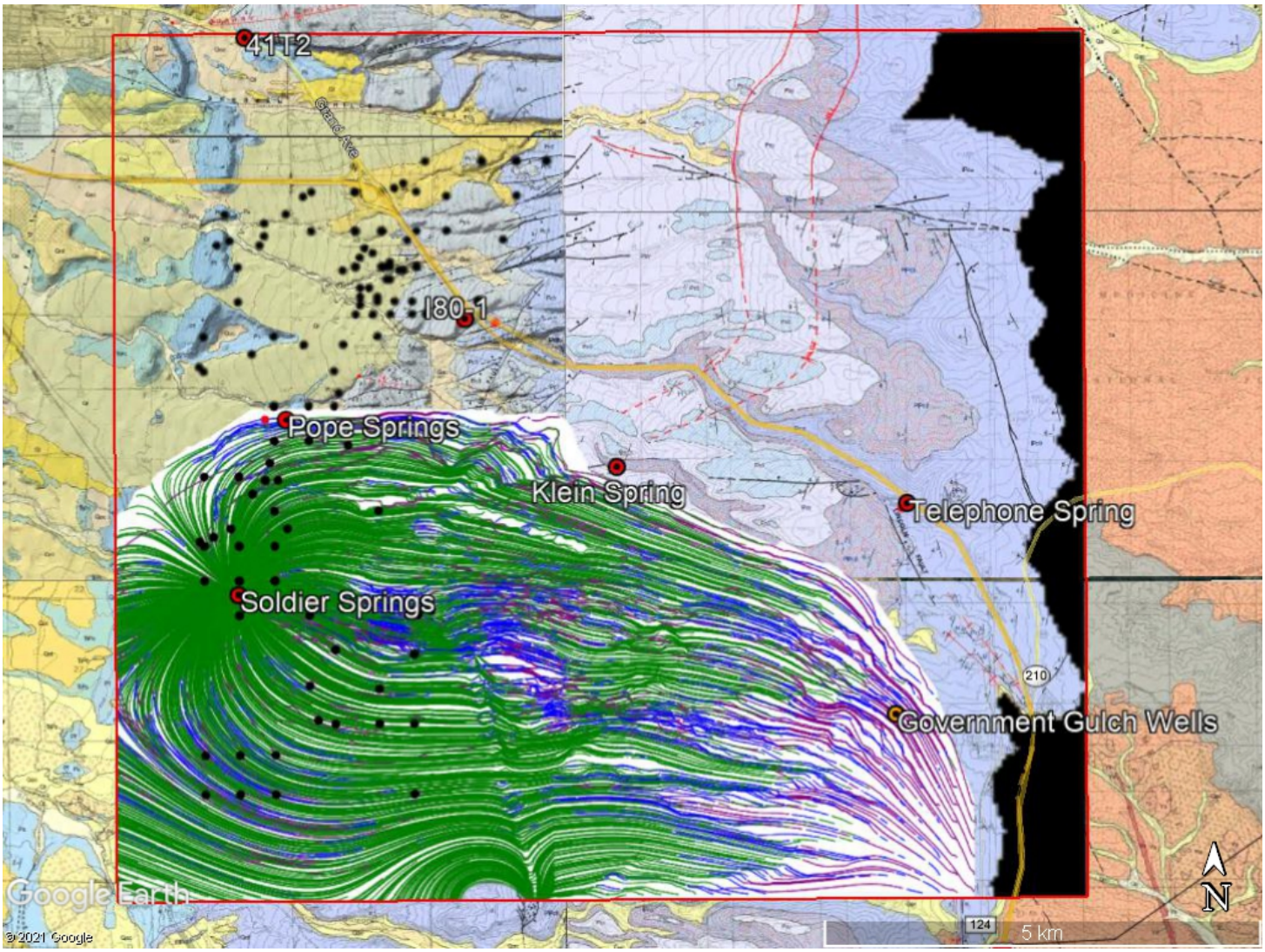

Figure 20.
M1, particle flow paths captured by the Soldier Springs well overlain in Google Earth on WGS geologic maps. Groundwater model domain outlined in red, the black on the east side of the model indicates cells that are "turned off." Black dots indicate SEO permitted private wells. Path line colors represent different layers of the model: purple indicates particles are in HL4, blue indicates particles are in HL3, and green indicates particles are in HL2. The capture zone of Soldier Springs does not intersect the I-80 corridor.

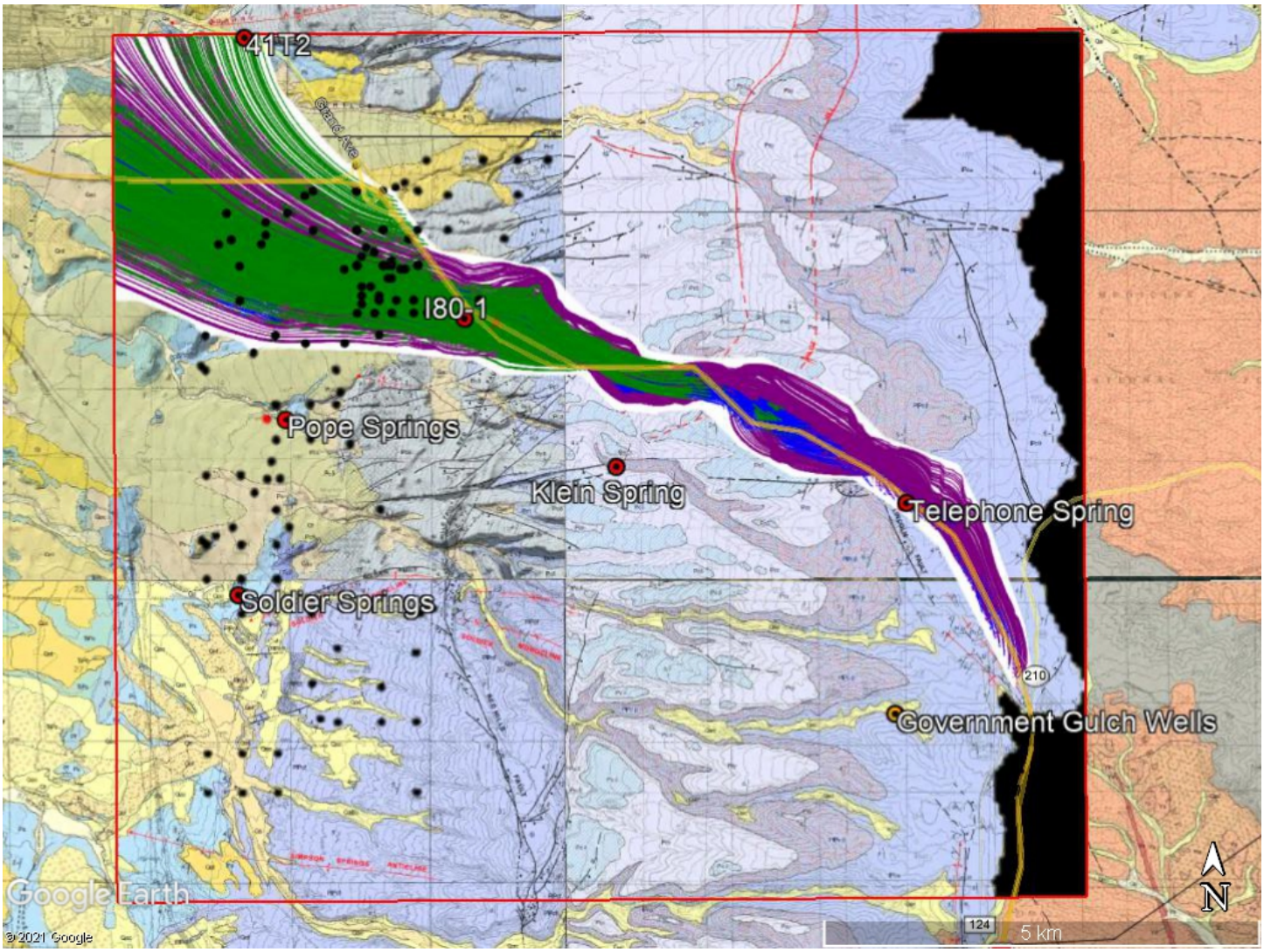

Figure 21.
M1, particle flow paths from release at points on and surrounding I-80 overlain in Google Earth on WGS geologic maps. Groundwater model domain outlined in red, the black on the east side of the model indicates cells that are “turned off.” Black dots indicate SEO permitted private wells. Path line colors represent different layers of the model: purple indicates particles are in HL4, blue indicates particles are in HL3, and green indicates particles are in HL2. The particle tracking shows spills on the interstate pose little threat to Soldier Springs, but flow directly under many privately owned wells.

Conclusions:

This report details the culmination of a two year project to collect and transform data from an airborne geophysical survey into a groundwater flow model of the Casper Aquifer within Albany County and in the vicinity Laramie, WY. The overall goal of this study is to integrate new geophysical data with existing geologic and hydrologic knowledge of the Casper Aquifer to better understand the flow of groundwater within the exposed section of the Casper and Fountain Formations. This improved understanding will help to create more informed plans to protect the City of Laramie and surrounding Albany County residents' water sources from possible spills on Interstate 80.

During the first year of this study airborne electromagnetic (AEM) and airborne magnetic (Aeromag) data were collected. The Aeromag data informed our knowledge of the type of rock in the basement, which is indicative of deep structure that can cause pathways for groundwater movement in the overlying sedimentary layers. The AEM data were processed and run through a spatially constrained inversion to create depth profiles of resistivity throughout the survey area. Since relative changes in resistivity are correlated with increases or decreases in porosity and permeability, this inversion provided new understanding of depths and layers that allow for more water movement within the aquifer than others. For more details on the progress made in year one, see the interim report (Carr & Smith, 2020).

In the second year of the project, the laterally extensive hydrogeophysical layers were picked in the AEM data. These layers are defined by sharp changes in the inverted resistivity. Extrapolating these layer elevations to the larger groundwater model grid and correlating resistivities to hydraulic conductivities, allowed the direct incorporation of the AEM data into a groundwater flow model. Hydrologic properties based on geophysical log measurements as well as previous studies on the aquifer are assigned and carefully altered within each hydrogeophysical layer until a model that most closely represents historic hydraulic head measurements is created. Particle tracking on this finalized model was run to understand how particles released near the interstate corridor would flow if they reached the water table.

The culmination of this geophysical and hydrologic modeling effort has led to three major conclusions about the flow of groundwater within the mountain front of the Casper Aquifer:

1) Deep basement structure and surface mapped faults have a variety of influences on groundwater flow within the aquifer. The sharp change in resistivity between the basement rock and overlying sedimentary formations in the AEM data show that areas where the basement topography changes in slope generally leads to lower resistivity in the overlying hydrogeophysical layers. Areas of decreases in resistivity are interpreted as areas of higher horizontal and vertical hydraulic conductivities, generally mapped as large structure such as monoclines in the WGS geologic maps. These deep structures seen on both the WGS maps and

in the AEM data are also mapped as highs in the aeromag data, indicating changes in the type of basement rock highlight areas of increased structural complexity in the overlying sedimentary aquifer. Conversely, areas in which there are a high density of surface mapped faults are generally correlated to areas with increases in resistivity in the AEM data. Furthermore, the addition of low K faults acting as barriers to horizontal groundwater flow in the groundwater model are key to the replication of historic hydraulic head data. The groundwater model additionally showed that these faults do not obstruct vertical flow, and sometimes allow more movement between layers due to the vertical hydraulic conductivity being larger than the horizontal. Both the AEM data and groundwater model elucidated the importance of these two structural elements in controlling the movement of water within the Casper Aquifer and inform our understanding of groundwater movement in areas outside of the groundwater model domain.

2) The 2005 hydraulic head contour map gave general indications of direction of flow within the aquifer. However, the creation of a model with added complexity and replication of historic hydraulic head data allows for a much more detailed understanding of particle movement in the aquifer. Particle tracking software, MODPATH 7, was run on the groundwater model to track the particles whose flow paths end at the Soldier Springs wells and the direction of flow of particles released on the Interstate. The first of which shows that the extent to which Soldier Springs pulls water, at current average pumping rates, is not large enough to pull water from the Interstate 80 corridor. This is good news as it suggests that the Soldier Springs municipal well fields are not currently vulnerable to spills from the interstate. The second MODPATH model additionally shows that no particles released near the Interstate are captured by the Soldier Pumping well. However, these pathways directly underlie many Albany County resident privately owned wells, leaving these residents vulnerable to spills should they reach the water table.

3) Understanding from where recharge to the aquifer comes is important for predictions of both the vulnerability of the aquifer in the changing climate of the West, and the likelihood of contaminants on the Interstate infiltrating our municipal source of water. The groundwater modeling effort showed that the replication of historic hydraulic head data was only possible if the majority of recharge to the aquifer is added at the higher elevated areas of the model. If more recharge was adding in the lower portion of the model, hydraulic head levels would be much higher in the valley. But if no recharge was added to these areas the model was also incorrect. This indicates that some recharge is necessary in the lower area of the mountain front, but that little water or snowmelt at the surface near the bottom of the interstate 80 corridor reaches the water table. This is good news for spills on the Interstate, as it suggests these contaminants would be unlikely to infiltrate enough of the unsaturated portion of the aquifer to reach the water table. However, due to the varying densities of possible

contaminants, their infiltration into the unsaturated zone is most likely different than that of water. A groundwater transport model would best predict how common contaminants might infiltrate and move through the aquifer.

Transforming borehole and airborne geophysical data into a groundwater model created a better understanding of how water enters, moves through, and exits our local aquifer system. This study showed the relative safety of Soldier Springs from pumping contaminants near the Interstate 80 corridor, and that little water in the lower regions of the aquifer reaches the water table.

Recommendations:

1) Since all particles released in the groundwater model along the interstate corridor were funneled to the northwest of the model, the I-80 monitoring wells are directly in line to monitor this area of concern. We recommend that these wells should be used to monitor water quality, and that additional monitoring wells should be drilled in the vicinity of the privately owned wells to best keep county residents aware of water quality issues.

2) The groundwater model was run with little pumping included at Pope Springs. Because of this, the cone of depression was not large enough to capture many particles. We recommend continuing to limit pumping at Pope Springs as it is likely that increasing the pumping out of these wells would draw water from the interstate, creating more concern for municipal water contamination.

3) A logical next step from this modeling effort is the creation of a groundwater transport model to predict how different contaminants might flow in the unsaturated zone and possibly interact with the aquifer in light of the flow paths indicated in this study.

References:

Bakker, M., Post, V. ., Langevin, C. D., Hughes, J. D., White, J. T., Starn, J. J., & Fienen, M. N. (2016). Scripting MODFLOW model development using Python and FloPy. *Groundwater*, *54*(5), 733–739.

Bakker, M., Post, V., Langevin, C. D., Hughes, J. D., White, J. T., Leaf, A. T., … Fienen, M. N. (2021). *FloPy v3.3.4 — release candidate: U.S. Geological Survey Software Release, 18 February 2021*. U.S. Geological Survey. Retrieved from http://dx.doi.org/10.5066/F7BK19FH

Borradaile, G. J. (1988). Magnetic susceptibility, petrofabrics and strain. *Tectonophysics*, *156*(1), 1–20. https://doi.org/https://doi.org/10.1016/0040-1951(88)90279-X

Carr, B., & Smith, E. (2020). *Airborne Electromagnetic Geophysical (AEM) Study along the I-80 Corridor and Municipal Wellfields within Albany County near Laramie, WY*. Laramie, WY.

e-Permit. (n.d.). Retrieved July 22, 2021, from http://seoweb.wyo.gov/e-Permit/common/login.aspx?ReturnUrl=%2Fe-Permit%2F

GeoScene3D Builder. (2021). Risskov, Denmark: I-GIS A/S.

Hubbard, S. S., & Linde, N. (2011). *Hydrogeophysics*.

Hughes, J. D., Langevin, C. D., & Banta, E. R. (2017). Documentation for the MODFLOW 6 framework: U.S. Geological Survey Techniques and Methods. In *Book 6* (p. 40). U.S. Geological Survey. Retrieved from https://doi.org/10.3133/tm6A57

Huntoon, P. W. (1985). FAULT SEVERED AQUIFERS ALONG THE PERIMETERS OF WYOMING ARTESIAN BASINS. *Ground Water*, *23*(2), 176–181. https://doi.org/10.1111/j.1745-6584.1985.tb02790.x

Huntoon, P. W., & Lundy, D. A. (1979). Fracture-controlled ground-water circulation and well siting in the vicinity of Laramie, Wyoming. *Groundwater*, *17*(5), 463. https://doi.org/10.1111/j.1745-6584.1979.tb03342.x

Langevin, C. D., Hughes, J. D., Banta, E. R., Niswonger, R. G., Panday, S., & Provost, A. M. (2017). Documentation for the MODFLOW 6 Groundwater Flow Model: U.S. Geological Survey Techniques and Methods. In *Book 6* (p. 197). U.S. Geological Survey. Retrieved from https://doi.org/10.3133/tm6A55

Langevin, C. D., Hughes, J. D., Banta, E. R., Provost, A. M., Niswonger, R. G., & Panday, S. (2021). *MODFLOW 6 Modular Hydrologic Model version 6.2.1: U.S. Geological Survey Software Release, 18 February 2021*. U.S. Geological Survey. Retrieved from https://doi.org/10.5066/F76Q1VQV

MATLAB: R2021a. (2021). Natick, Massachusetts: The Mathworks, Inc.

Office, W. W. D. (n.d.). Wyoming Water Facts. Retrieved from https://waterplan.state.wy.us/waterfacts.html

Pollock, D. W. (2016). *User guide for MODPATH Version 7—A particle-tracking model for MODFLOW: U.S. Geological Survey Open-File Report 2016–1086*.

https://doi.org/http://dx.doi.org/10.3133/ofr20161086

PRISM Gridded Climate Data. (2004). PRISM Climate Group, Oregon State University. Retrieved from http://prism.oregonstate.edu

Taboga, K. (2005). *Plate 10-2 Potentiometric Surface Map of Casper Aquifer*. Laramie Water Management Study, Level II Wyoming Water Development Commission.

Ver Ploeg, A.J., and McLaughlin, J. F. (2009). *Geologic Map Of The Pilot Hill Quadrangle, Albany County, Wyoming*. Wyoming State Geological Survey Map Series 89, scale 1:24,000.

Ver Ploeg, A.J., and McLaughlin, J. F. (2010). *Preliminary Geologic Map Of The Sherman Mountains West Quadrangle, Albany County, Wyoming*. Wyoming State Geological Survey Open File Report 10-3, scale 1:24,000.

Ver Ploeg, A. J. (2007). *Geologic Map Of The Red Buttes Quadrangle, Albany County, Wyoming*. Wyoming State Geological Survey Map Series 76, scale 1:24,000.

Ver Ploeg, A. J. (2009). *Revised Geologic Map Of The Laramie Quadrangle, Albany County, Wyoming*. Wyoming State Geological Survey Map Series 50, version 1.0, scale 1:24,000.

Viezzoli, A., Christiansen, A. V., Auken, E., & Sørensen, K. (2008). Quasi-3D modeling of airborne TEM data by spatially constrained inversion. *Geophysics*, *73*(3), F105–F113.

Wittman Hydro Planning Associates. (2008). *Casper Aquifer Protection Plan*. Laramie, WY.

Appendices:

1) Appendix 1: 3D hydrogeophysical model
2) Appendix 2: AEM and extrapolated hydrogeophysical layer top and bottom elevation topography

Appendix 1: 3D hydrogeophysical model

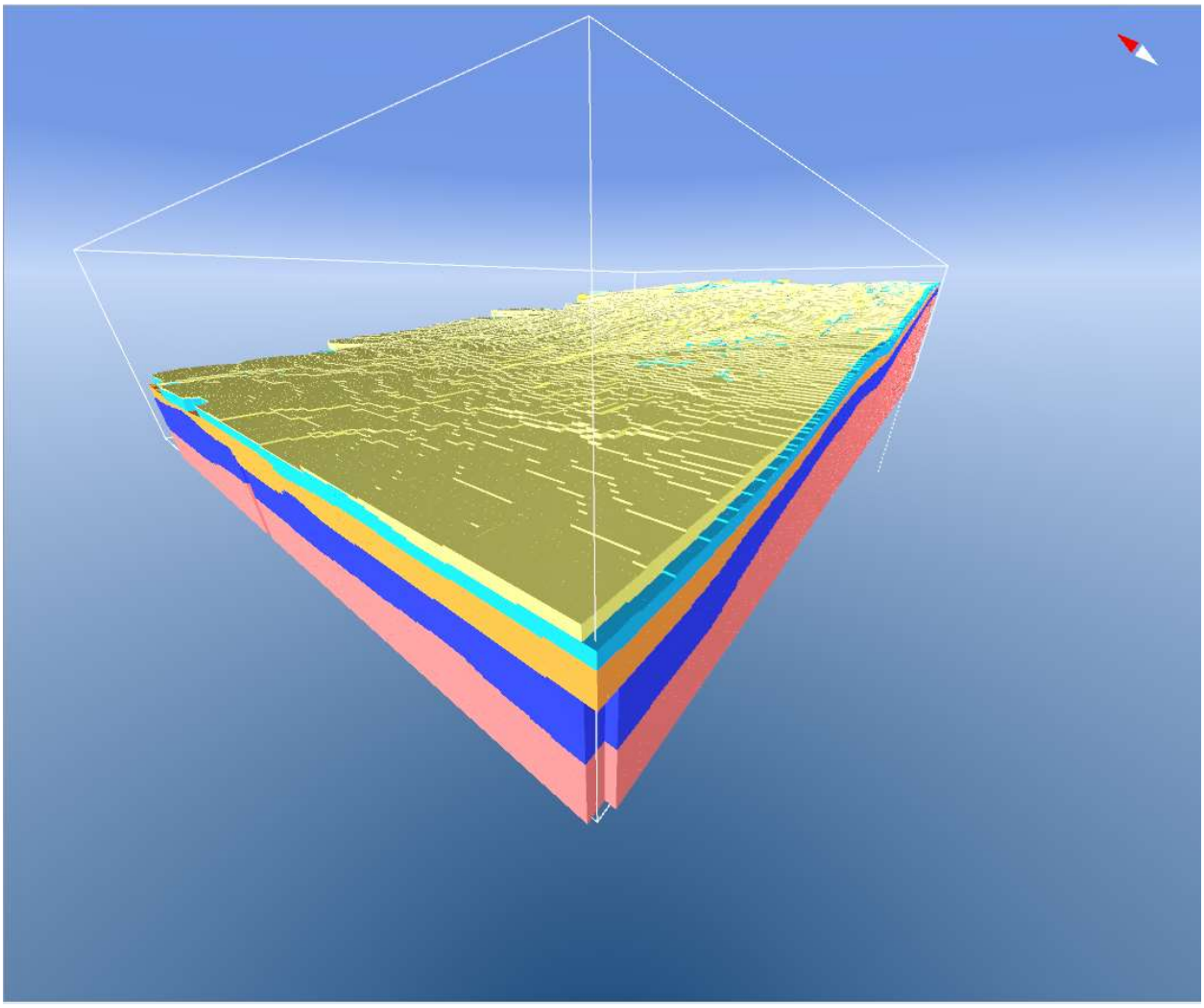

Figure 1.

View of 3D model of aquifer layers in GeoScene3D from the SW looking to the NE. Yellow is HL1, light blue is HL2, orange is HL3, dark blue is HL4, and pink in underlying basement. Vertical Scale 2:1. This view shows the layered natured of the aquifer.

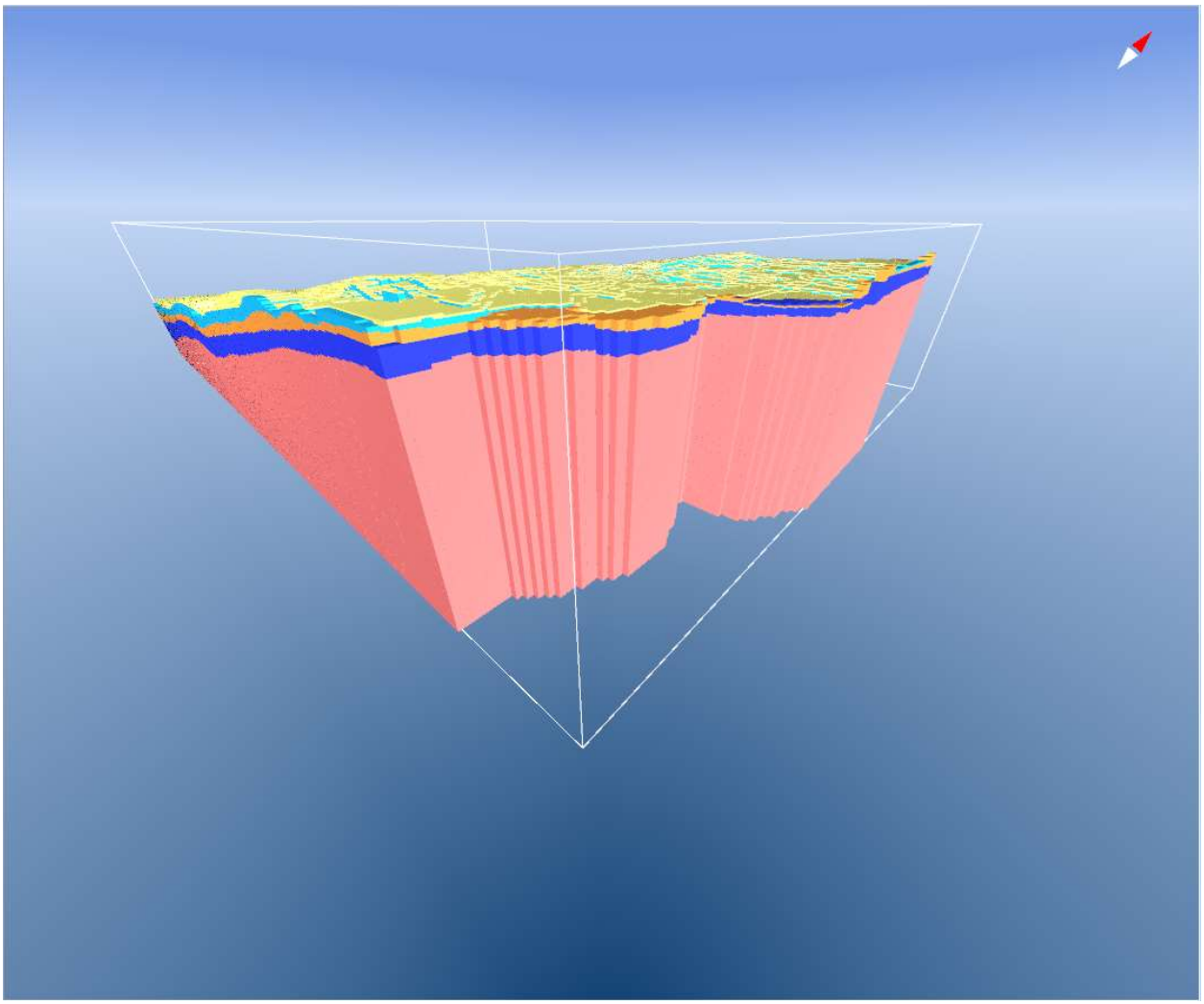

Figure 2.

View of 3D model of aquifer layers in GeoScene3D from the SE looking to the NW. Yellow is HL1, light blue is HL2, orange is HL3, dark blue is HL4, and pink in underlying basement. Vertical Scale 2:1. This view shows the lateral extent of HL4 throughout the aquifer.

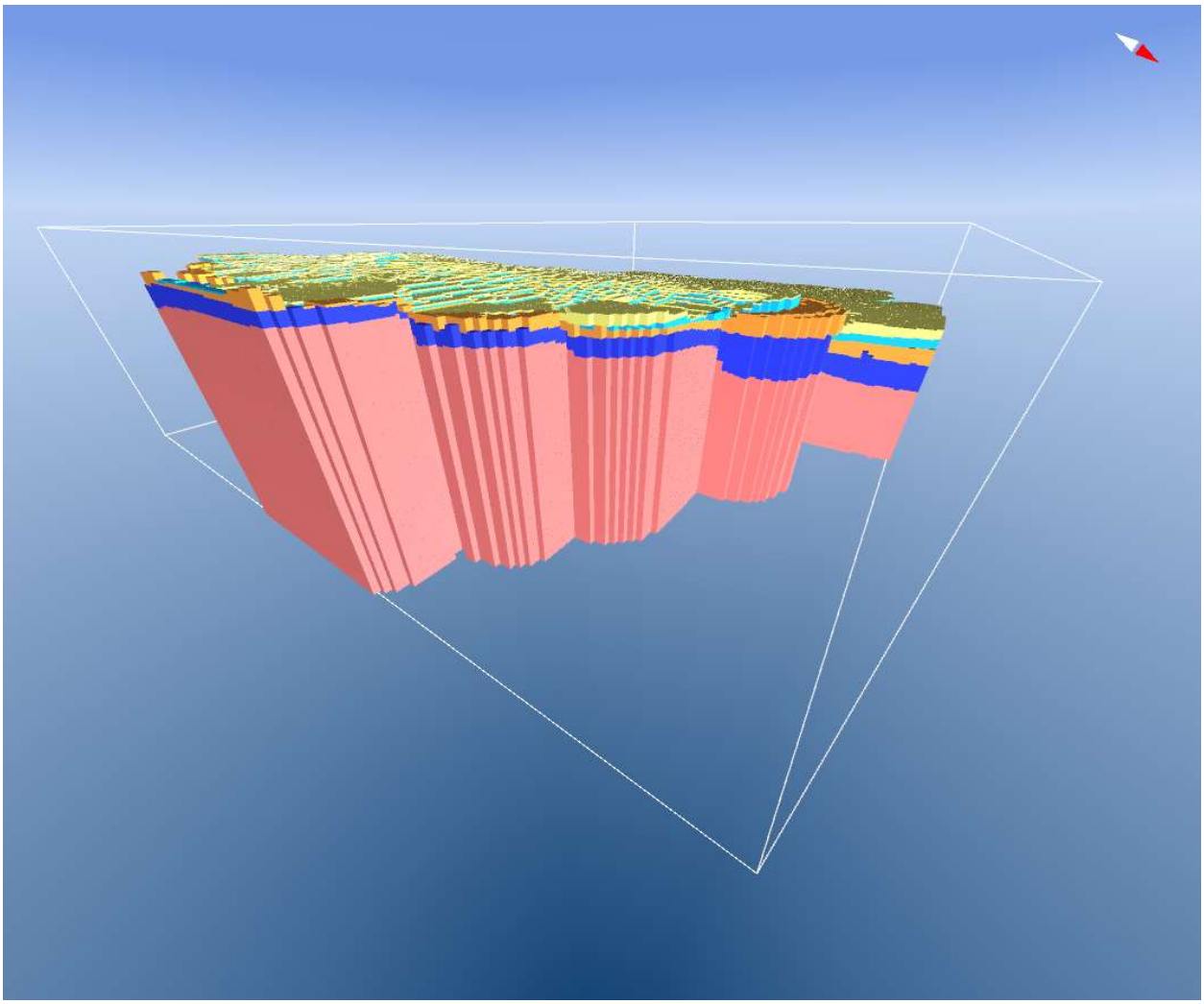

Figure 3.

View of 3D model of aquifer layers in GeoScene3D from the NE looking to the SW. Yellow is HL1, light blue is HL2, orange is HL3, dark blue is HL4, and pink in underlying basement. Vertical Scale 2:1. This view additionally shows the lateral extent of HL4 throughout the aquifer.

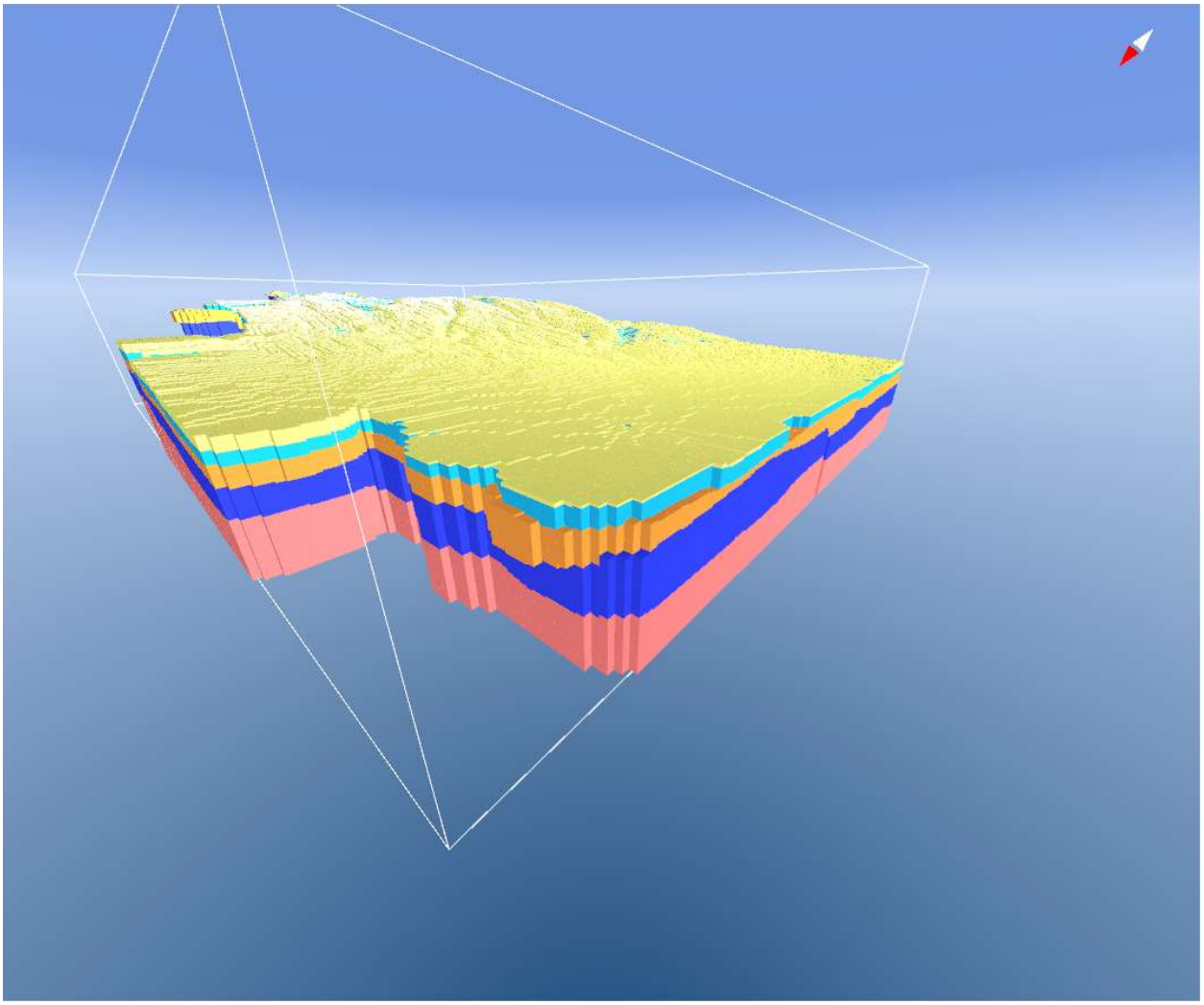

Figure 4.

View of 3D model of aquifer layers in GeoScene3D from the NW looking to the SE. Yellow is HL1, light blue is HL2, orange is HL3, dark blue is HL4, and pink in underlying basement. Vertical Scale 2:1. This view shows the change in thickness of HL3 near the city well fields Pope and Soldier Springs.

Appendix 2: AEM and extrapolated hydrogeophysical layer top and bottom elevation topography

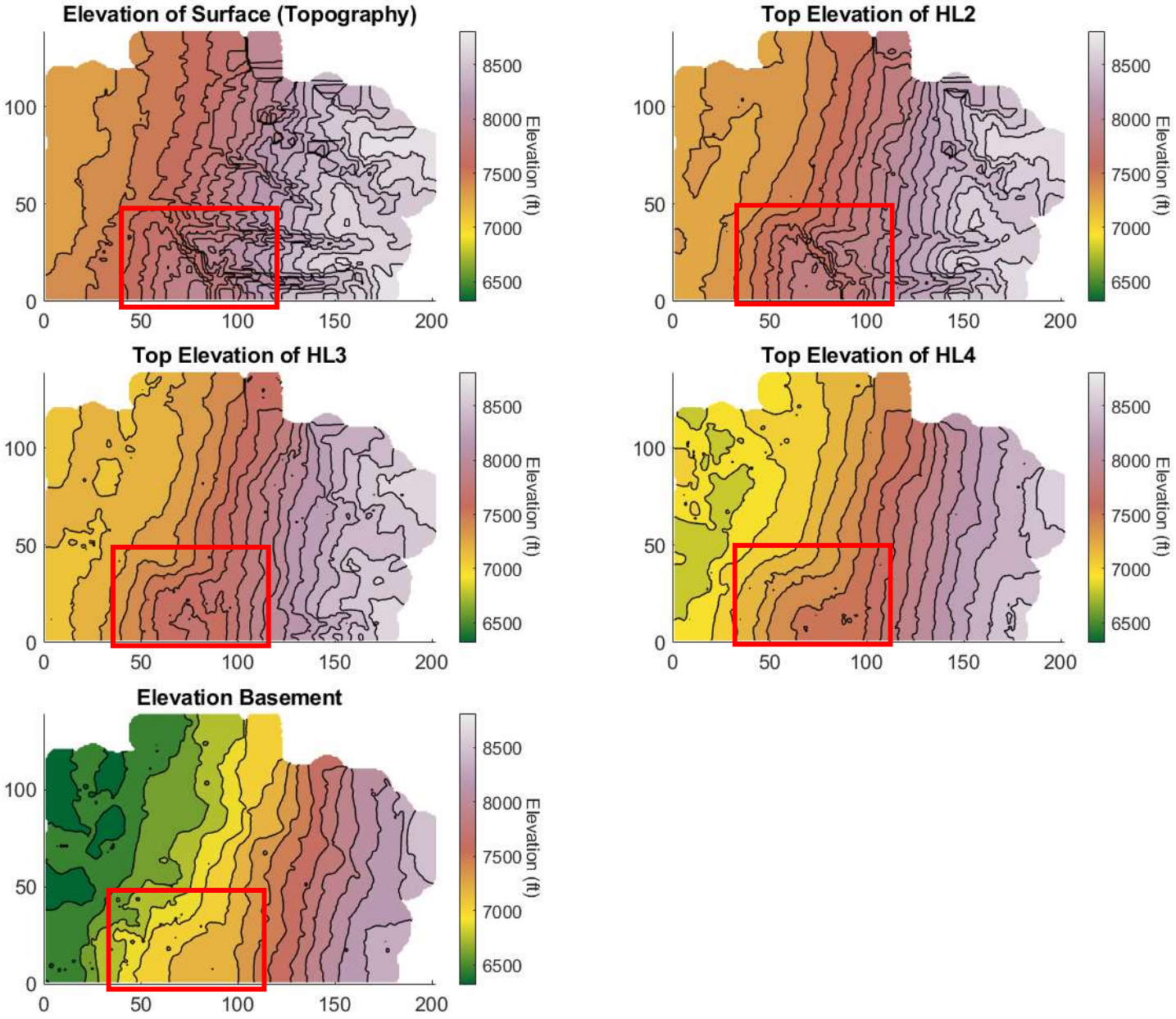

Figure 1.

Elevation of each layer picked in GeoScene3D. Change in basement slope circled in red visible through all layers. This shows the importance of basement topography on overlying hydrogeophysical layers.

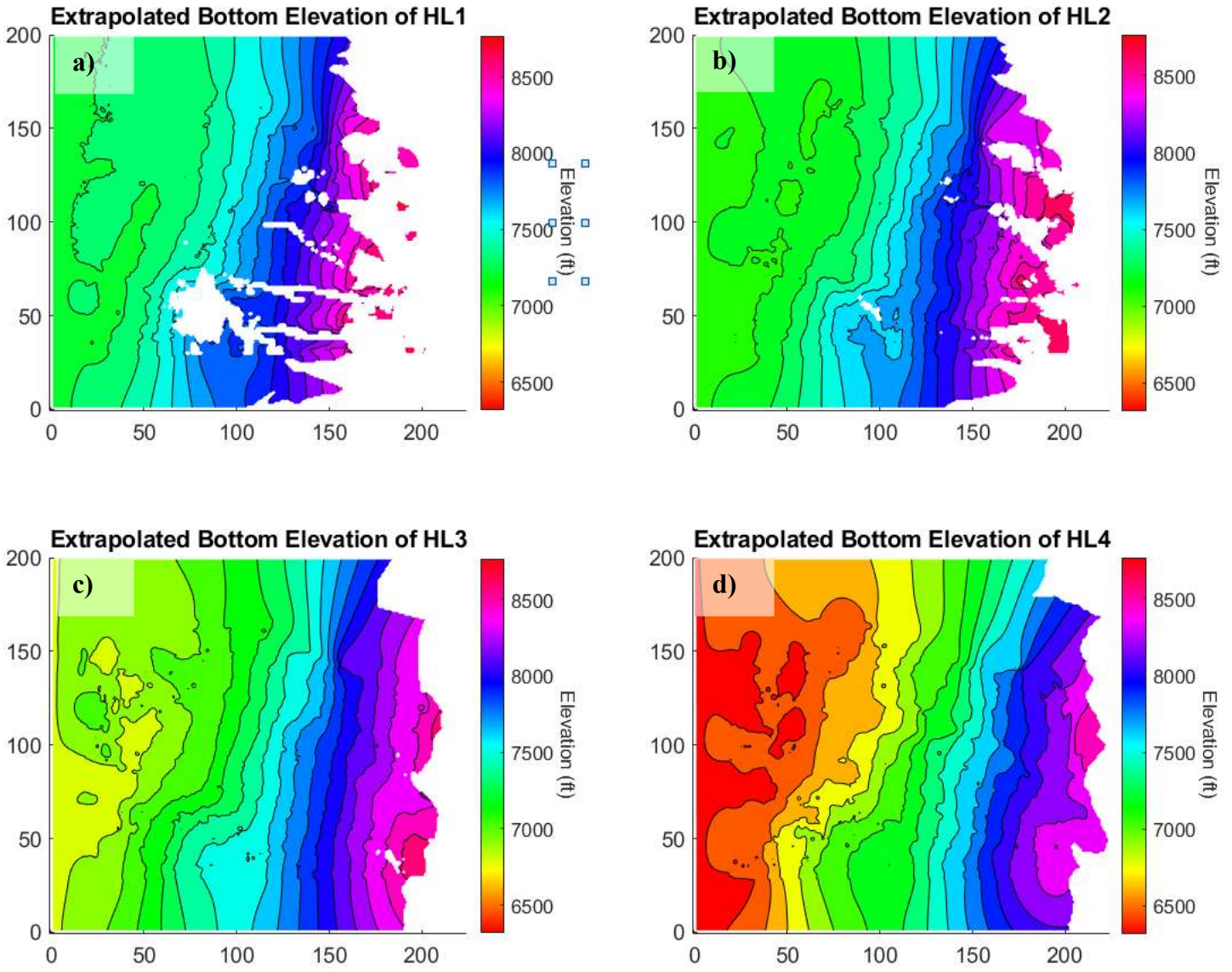

Figure 2.

Extrapolated elevation of each hydrogeophysical layer, of which a) is used to define top of the groundwater model, and b) – d) are used for model layers HL2 - HL4 bottom elevations from top to bottom, respectively.